Electronic Supplementary Material (ESI) for ChemComm.
This journal is © The Royal Society of Chemistry 2023

Stimuli-responsive assembly and disassembly of anionic suprasomes with tunable antibacterial activity

Biswa Mohan Prusty,[a] Rama Karn,[b] Anjali Patel,[b] Priyanka Mazumder,[b] Sachin Kumar,[c] and Debasis Manna*[ab]

[a]Department of Chemistry, Indian Institute of Technology Guwahati, Assam-781039, India
[b]Centre for the Environment, Indian Institute of Technology Guwahati, Assam-781039, India
[c]Department of Bioscience and Bioengineering, Indian Institute of Technology Guwahati, Assam-781039, India

S. No.	Contents	Pages
1	General information	S2
2	Synthesis and characterization of amphiphiles	S2-4
3	Formation of micelle and suprasomes	S4
4	Measurements of hydrodynamic diameters	S4-11
5	Stability of suprasomes	S11-14
6	Isothermal titration calorimetry measurements	S14-15
7	Morphology studies of micelles and suprasomes by TEM and AFM analyses	S15
8	Effect of metal ions on hydrodynamic diameter and surface potential	S16-17
9	Morphology studies of nanoaggregates after Zn^{2+} addition	S17-19
10	Nile Red-based kinetics experiment	S20-21
11	Drug encapsulation and release studies	S21-22
212	Antimicrobial activity assessment	S22-26
13	Bacterial cell morphology analysis by FESEM	S27
14	Blood cells cytocompatibility test	S28-29
15	Cell viability analysis	S29-30
16	Membrane depolarization assay	S30
17	Propidium iodide uptake assay	S31-32
18	References	S34

Experimental section

1. General information:

The benzimidazole, 1-bromododecane, methyl iodide, propidium iodide, carboxyfluorescein, and diacetate-succinamide ester (cFDA-SE) were purchased from Sigma-Aldrich. The dialysis membrane-110 and all the bacterial culture media were procured from HImedia. Tetracycline and β-cyclodextrin (β-CD) were purchased from TCI. Benzimidazolium and imidazolium derivatives were purified by column chromatography and thin-layer chromatography (TLC). The ^{13}C NMR and ^{1}H NMR were recorded at 600 MHz with a Brucker spectrometer to observe the chemical shift, and for this purpose, DMSO-d_6 and $CDCl_3$ were used as the internal solvent. Multiplicities of the NMR spectra were reported as m (multiplet), d (doublet), s (singlet).

2. Synthesis and characterization of amphiphiles:

2.1. Synthesis of 1-dodecyl-3-methyl-1*H*-benzo[d]imidazol-3-ium iodide (C12mbm) — To a stirring solution of benzimidazole (1 mmol) in CH_3CN, KOH was added (1 mmol), and the reaction mixture was continued to stir for 1-2 h at room temperature. After that, 1-bromododecane (2 mmol) was added, and the reaction mixture was heated under reflux conditions for 24 hours. The progress of the reaction was monitored by TLC. After maximum

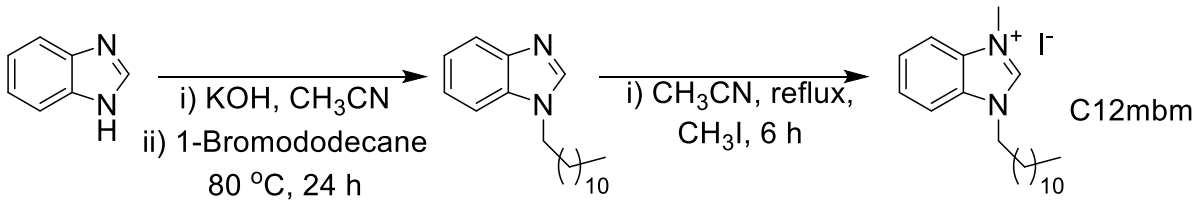

Scheme S1. Synthetic routes to 1-dodecyl-3-methyl-1*H*-benzo[d]imidazol-3-ium iodide (C12mbm).

consumption of benzimidazole, the reaction mixture was cooled down to room temperature, and unused KOH was removed by filtration. Then the organic solvent was removed under reduced pressure to yield an oily crude product. The mixture was purified through silica gel column chromatography with a solvent gradient system of 5–15% ethyl acetate in hexane to afford 1-dodecyl-1*H*-benzo[d]imidazole. After that, to a stirring solution of 1-dodecyl-1*H*-benzo[d]imidazole (1 mmol) in acetonitrile (inert condition), iodomethane (3 mmol) was added and refluxed until maximum consumption of 1-dodecyl-1*H*-benzo[d]imidazole (6 h). The progress of the reaction was monitored by TLC. Then the organic solvent was removed under reduced pressure to yield C12mbm.

The 1-dodecyl-1*H*-benzo[d]imidazole was characterized by HRMS (ESI), ^{1}H NMR, and ^{13}C NMR analysis. **^{1}H NMR (400 MHz, $CDCl_3$):** δ_{ppm} 7.88 (s, 1H), 7.82-7.80 (m, 1H), 7.41-7.38 (m, 1H), 7.32-7.29 (m, 1H), 7.28-7.25 (m, 1H), 4.15 (t, *J* = 7.1 Hz, 2H), 1.86 (m, *J* = 7.2 Hz, 2H), 1.32 (br, 4H), 1.24 (br, 4H), 0.88 (t, *J* = 6.8 Hz, 3H). **^{13}C NMR (126 MHz, $CDCl_3$):** δ_{ppm} 143.87, 142.91, 133.83, 122.77, 122.00, 120.36, 109.66, 45.12, 31.90, 29.82, 29.59, 29.51, 29.42, 29.32, 29.10, 26.83, 22.68, 14.11; HRMS (ESI) m/z: calculated for C19H30N2 $[M+H]^+$: **287.2482, found 287.2463.**

The C12mbm was characterized by HRMS (ESI), ^{1}H NMR, and ^{13}C NMR analysis. **^{1}H NMR (500 MHz, $CDCl_3$):** δ_{ppm} 11.07 (s, 1H), 7.73-7.70 (m, 4H), 4.57 (t, *J* = 7.5 Hz, 2H), 4.31 (s, 3H), 2.11-2.05 (m, 2H), 1.47-1.41 (m, 2H), 1.40-1.34 (m, 2H), 1.25 (br, 14H), 0.88 (t, *J* = 7.5 Hz, 3H). **^{13}C NMR (151 MHz, $CDCl_3$):** δ_{ppm} 142.37, 132.07, 131.16, 127.40, 127.38, 112.92, 112.88, 47.80, 33.93, 31.90, 29.59, 29.50, 29.38, 29.33, 29.03, 26.61, 22.69, 14.13; HRMS (ESI) m/z: calculated for C20H33N2 $[M]^+$: 301.2641, found 301.2638.

2.2. Synthesis of 1-dodecyl-3-methyl-1*H*-benzo[d]imidazol-3-ium iodide (C12mim) — To a stirring solution of imidazole (1 mmol) in CH_3CN, KOH was added (1 mmol), and the reaction mixture was continued to stir for 1-2 h at room temperature. After that, 1-bromododecane (2 mmol) was added, and the reaction mixture was heated under reflux conditions for 24 hours. The progress of the reaction was monitored by TLC. After maximum consumption of imidazole, the reaction mixture was cooled down to room temperature, and unused KOH was removed by filtration. Then the organic solvent was removed under reduced pressure to yield an oily crude product. The mixture was purified through a silica gel column

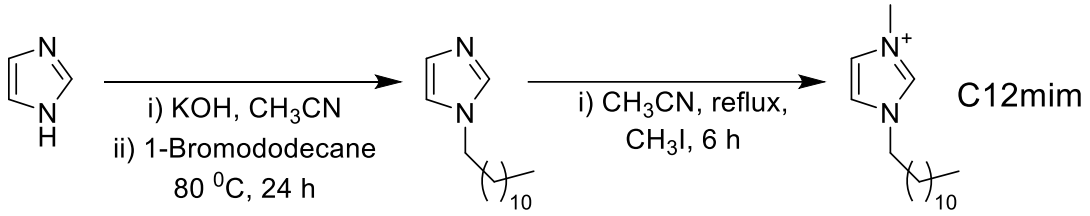

Scheme S2. Synthetic routes to 1-dodecyl-3-methyl-1*H*-benzo[d]imidazol-3-ium iodide (C12mim).

chromatography with a solvent gradient system of 5–15% ethyl acetate in hexane to afford 1-dodecyl-1*H*-imidazole. Thereafter, to a stirring solution of 1-dodecyl-1*H*-imidazole (1 mmol) in acetonitrile (inert condition), iodomethane (3 mmol) was added and refluxed until maximum

consumption of 1-dodecyl-1*H*-imidazole. The progress of the reaction was monitored by TLC. Then the organic solvent was removed under reduced pressure to yield C12mim.

The 1-dodecyl-1*H*-imidazole was characterized by HRMS (ESI), ^{1}H NMR, and ^{13}C NMR analysis. **^{1}H NMR (500 MHz, CDCl$_3$):** δ_{ppm} 7.45 (s, 1H), 7.05 (s, 1H), 6.90 (s, 1H), 3.91 (t, J = 7.3 Hz, 2H), 1.79-1.74 (m, 2H), 1.29 (br, 4H), 1.25 (br, 14H), 0.88 (t, J = 6.8 Hz, 3H). **^{13}C NMR (126 MHz, CDCl$_3$):** δ_{ppm} 136.94, 123.65, 121.99, 77.32, 77.07, 76.82, 50.34, 37.18, 31.89, 30.24, 29.58, 29.49, 29.37, 29.31, 28.98, 26.26, 22.66, 14.11; HRMS (ESI) m/z: calculated for C15H28N2 $[M+H]^+$: 237.2325, found 237.2301.

The C12mim was characterized by HRMS (ESI), ^{1}H NMR, and ^{13}C NMR analysis. **^{1}H NMR (126 MHz, CDCl$_3$):** δ_{ppm} 10.03 (s, 1H), 7.51 (s, 1H), 7.39 (s, 1H), 4.32 (t, J = 7.5 Hz, 2H), 4.13 (s, 3H), 1.93 (p, J = 7.4 Hz, 2H), 1.35-1.33 (br, 4H), 1.25 (br, 14H), 0.88 (t, J = 6.8 Hz, 3H). **^{13}C NMR (151 MHz, CDCl$_3$):** δ_{ppm} 136.94, 123.65, 121.99, 77.32, 77.07, 76.82, 50.34, 37.18, 31.89, 30.24, 29.58, 29.49, 29.37, 29.31, 28.98, 26.26, 22.66, 14.11; HRMS (ESI) m/z: calculated for C16H31N2 $[M+H]^+$: **252.2560, found 252.2531.**

2.3. Synthesis of sodium oleate — To a stirring solution of oleic acid in ethanol, NaOH was added and stirred for 4-5 h at room temperature. A white precipitate was formed, which was filtered and washed with ethanol to remove excess oleic acid. The filtered white precipitate was dried to get sodium oleate (NaOle).

3. Formation of micelle and suprasomes:

C12mbm (1 mM) and NaOle (1 mM) were added to 1 mL water in a clean vial and sonicated and vortexed for 15 min to form the micelles. Micelles were also prepared at different ratios of C12mbm and NaOle, such as 1:1 (composition A), 1:2 (composition B), and 1:5 (composition C). Then different concentrations of β-CD were added to the micellar system, vortexed for 5 min, and kept in the shaker at 180 rpm for 1 h to allow the conversion from micelles to suprasomes.

4. Measurements of hydrodynamic diameters:

Micelles were prepared in different compositions, and 1 mM β-CD was added to it and kept in the shaker at 180 rpm for 1 h, and then the hydrodynamic diameter was measured using Zetasizer Nano ZS90 (Malvern, Westborough, MA) instrument at 25 °C. β-CD concentration was increased by 1 mM after each measurement, and the same procedure was repeated to measure the hydrodynamic diameter of the suprasomes formed. A similar procedure was

followed to measure the effect of β-CD concentration on the zeta potential of the suprasomes. These measurements were performed for all the compositions.

Table S1. Selected compositions of the additives for further studies.

Compositions	Additives (molar ratio)
Composition A	C12mbm: NaOle: β-CD (1: 1: 10)
Composition B	C12mbm : NaOle: β-CD (1 : 2: 10)
Composition C	C12mbm : NaOle: β-CD (1 : 5: 10)
Composition D	C12mim : NaOle: β-CD (1 : 1: 10)

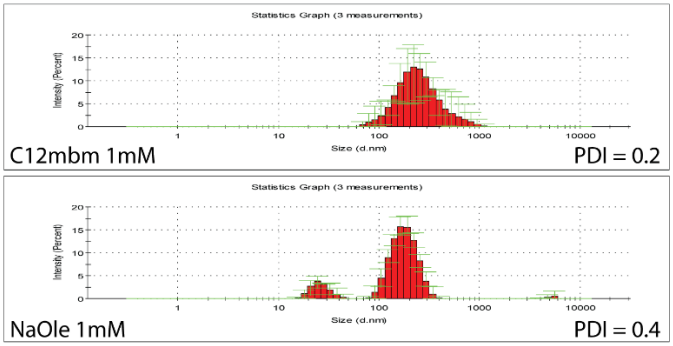

Fig. S1. Hydrodynamic diameters (d_H) of only C12mbm and NaOle.

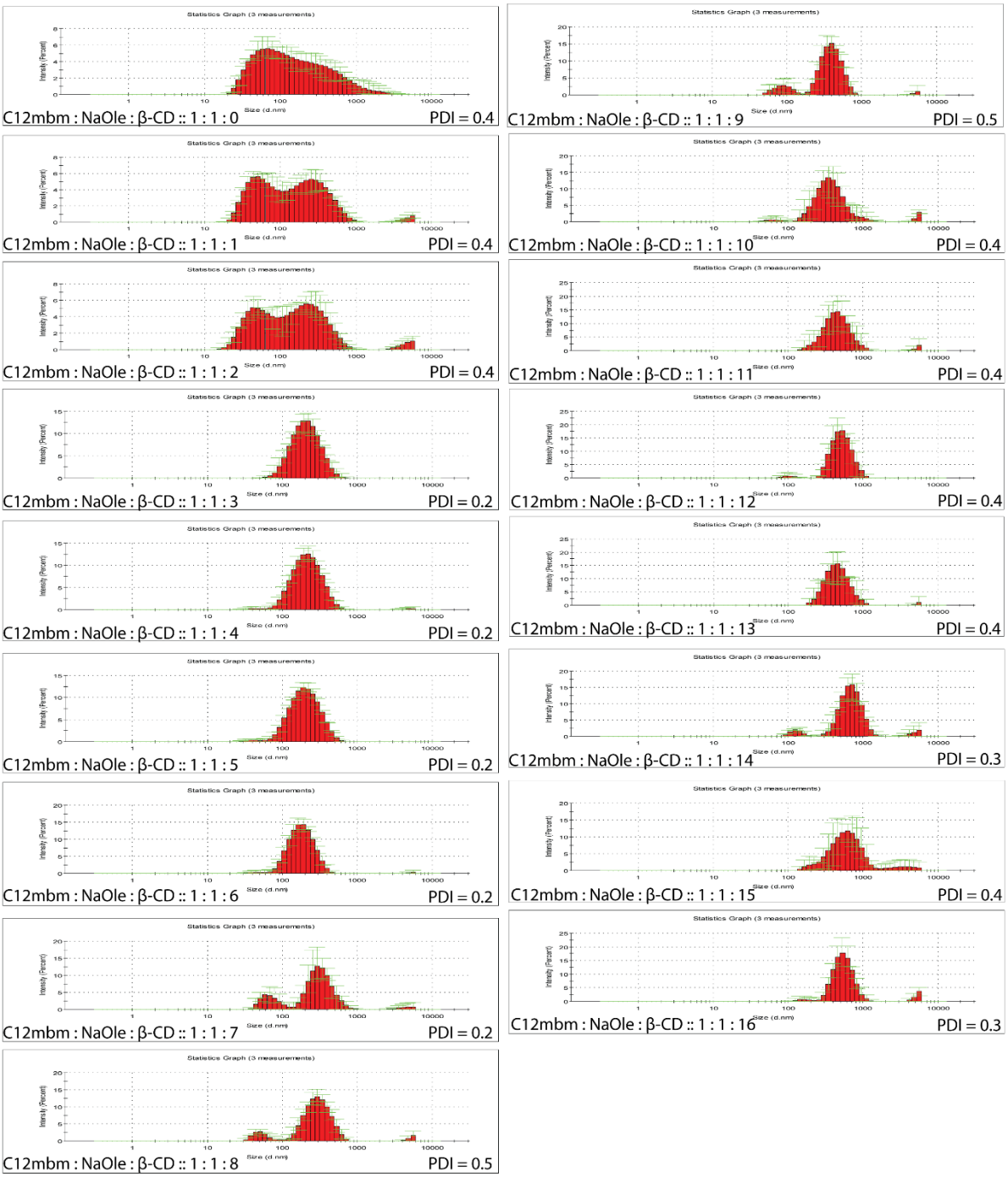

Fig. S2. Variation of hydrodynamic diameter of the C12mbm and NaOle (1: 1, C/C) at different concentrations of β-CD.

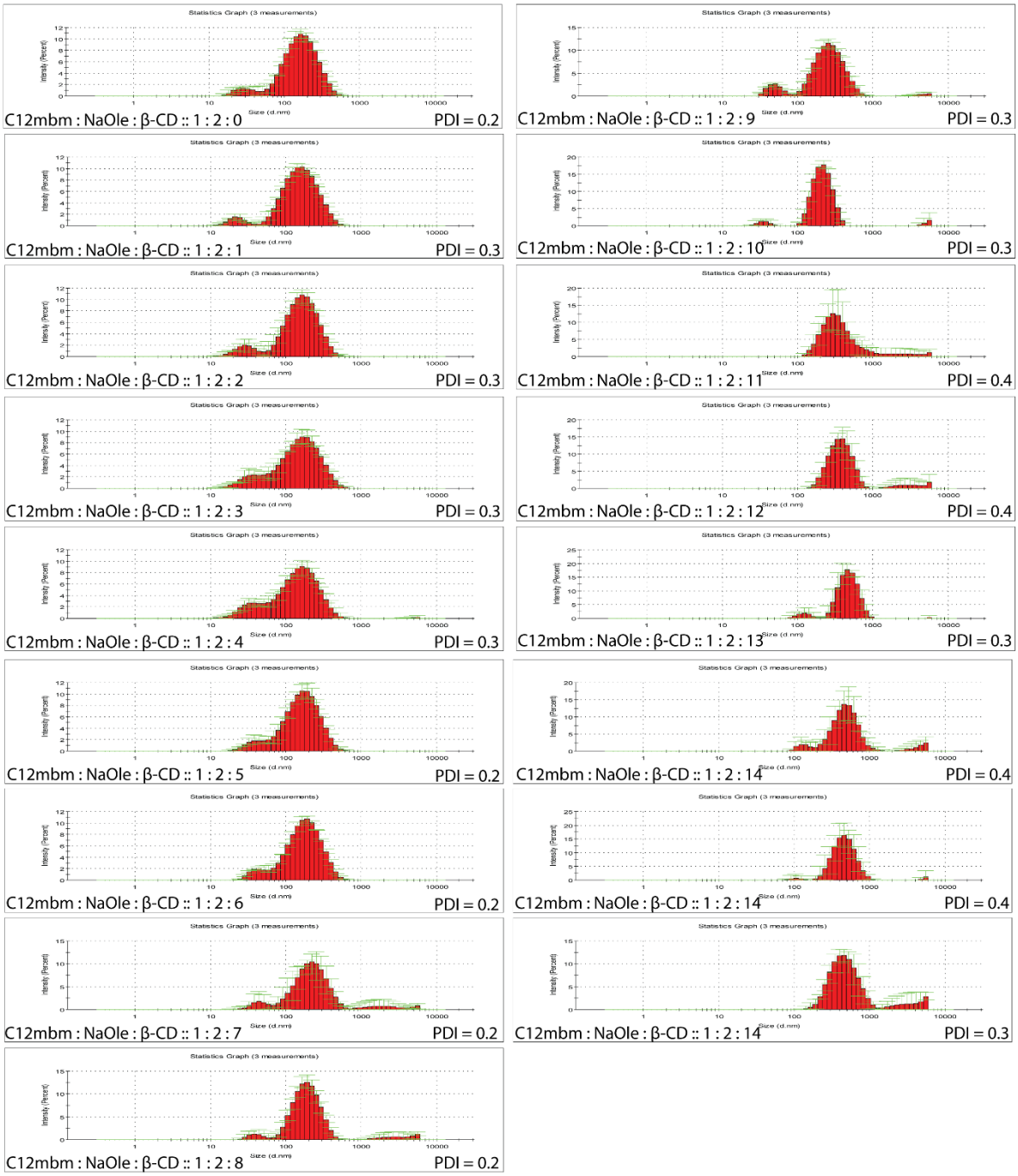

Fig. S3. Variation of hydrodynamic diameter of the C12mbm and NaOle (1: 2, C/C) at different concentrations of β-CD.

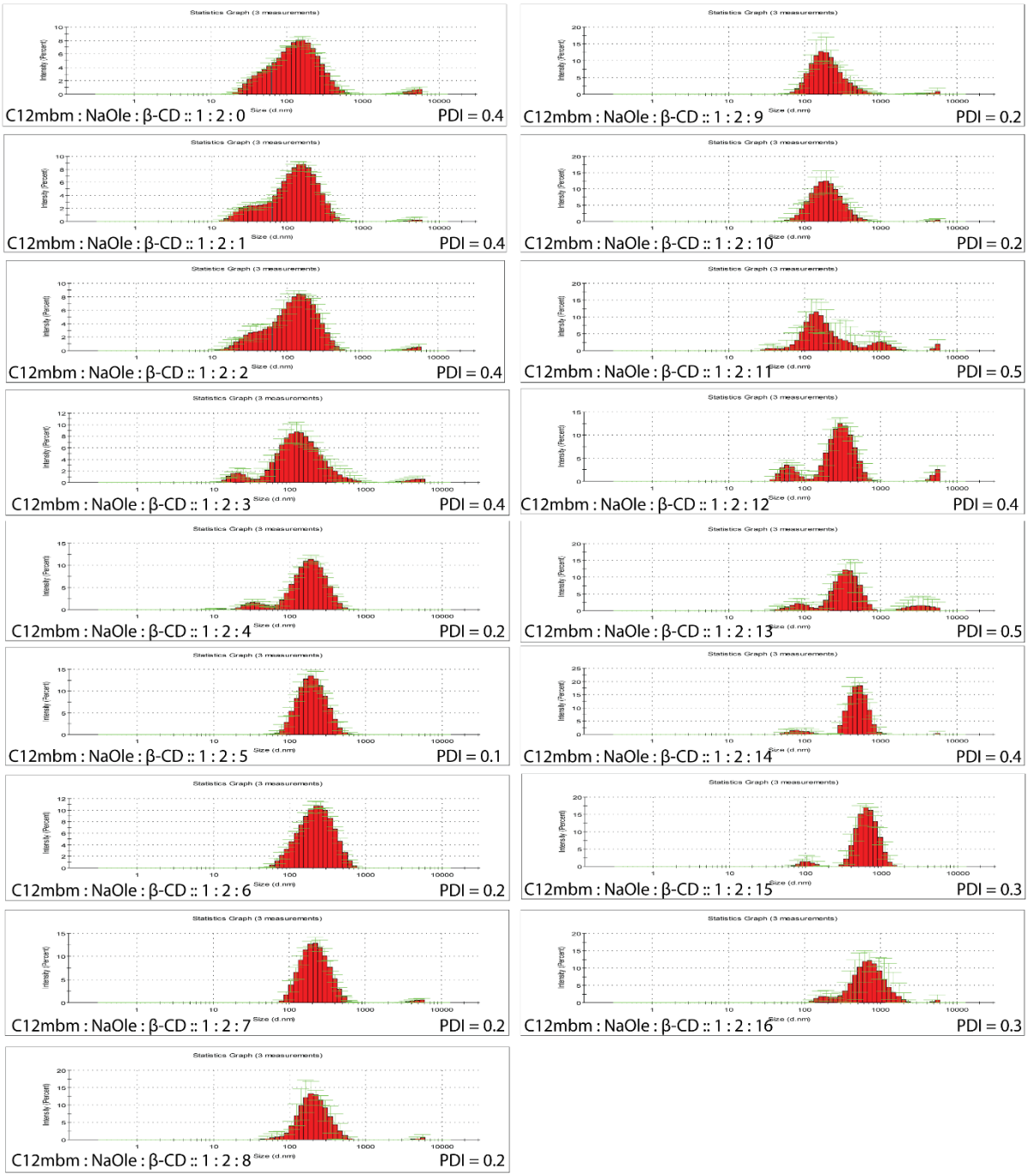

Fig. S4. Variation of hydrodynamic diameter of the C12mbm and NaOle (1: 5, C/C) at different concentrations of β-CD.

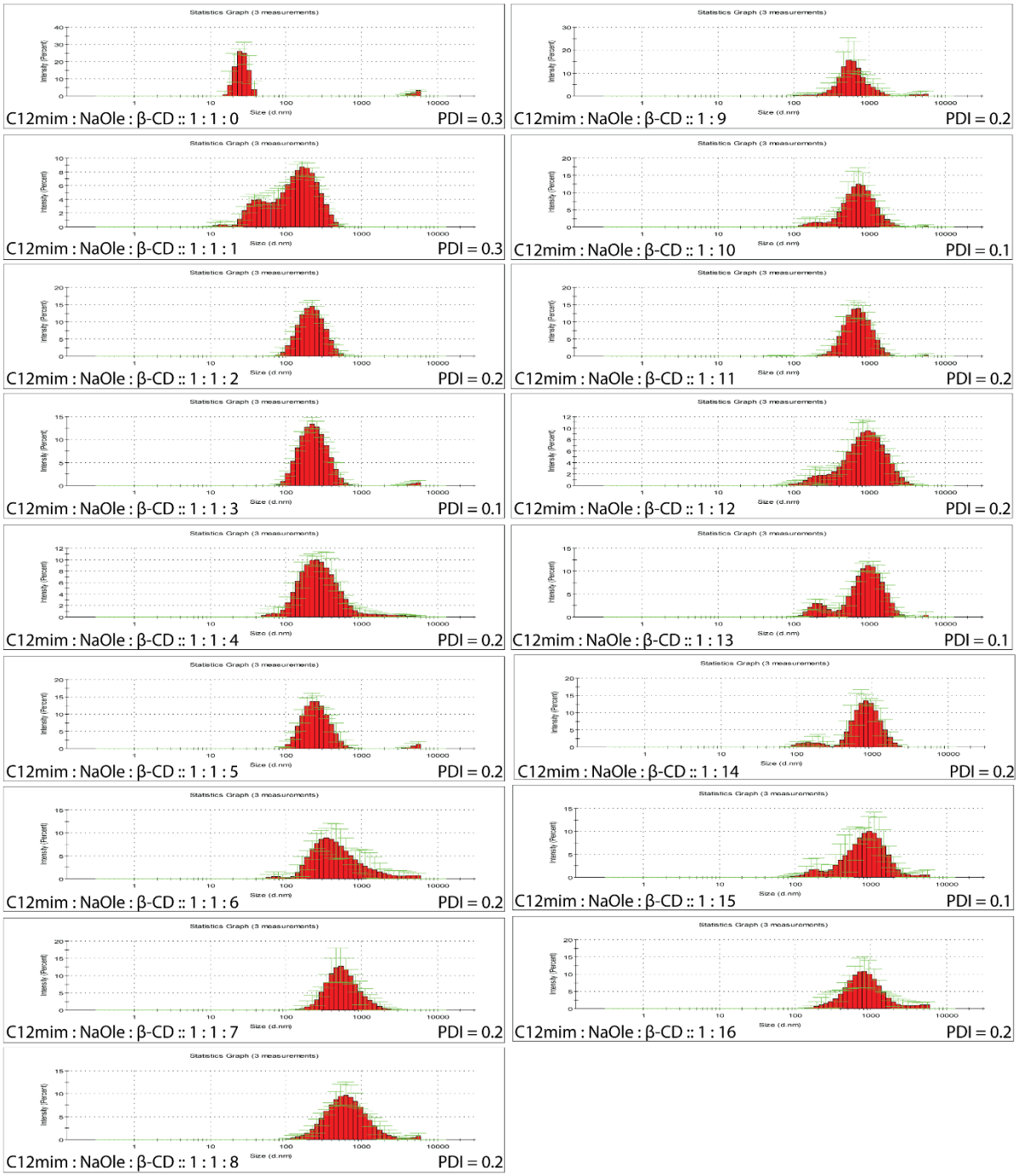

Fig. S5. Variation of hydrodynamic diameter of the C12mim and NaOle (1: 1, C/C) at different concentrations of β-CD.

Table S2. Variation of hydrodynamic diameter of the soluble aggregates at different concentrations of β-CD.

[β-CD]/ (mM)	Hydrodynamic diameter (nm)			
	(C12mbm : NaOle :: 1 mM : 1 mM)	(C12mbm : NaOle :: 1 mM : 2 mM)	(C12mbm : NaOle :: 1 mM : 5 mM)	(C12mim : NaOle :: 1 mM : 1 mM)
0	98.47 ± 1.9 (PDI = 0.4)	121.63 ± 1.6 (PDI = 0.2)	97.52 ± 0.5 (PDI = 0.4)	28.97 ± 2.7 (PDI = 0.3)
1	94.25 ± 1.6 (PDI = 0.4)	115.70 ± 0.8 (PDI = 0.3)	90.16 ± 2.0 (PDI = 0.4)	93.64 ± 1.7 (PDI = 0.3)
2	94.09 ± 1.4 (PDI = 0.4)	112.30 ± 0.5 (PDI = 0.3)	87.63 ± 0.9 (PDI = 0.4)	189.06 ± 3.9 (PDI = 0.2)
3	169.43 ± 1.2 (PDI = 0.2)	102.36 ± 2.2 (PDI = 0.3)	99.23 ± 0.4 (PDI = 0.4)	213.70 ± 2.0 (PDI = 0.1)
4	182.06 ± 0.8 (PDI = 0.2)	97.71 ± 1.8 (PDI = 0.3)	134.76 ± 1.7 (PDI = 0.2)	233.26 ± 0.6 (PDI = 0.2)
5	171.76 ± 2.9 (PDI = 0.2)	123.86 ± 1.0 (PDI = 0.2)	171.03 ± 1.3 (PDI = 0.1)	240.03 ± 4.1 (PDI = 0.2)
6	167.50 ± 3.8 (PDI = 0.2)	133.60 ± 1.6 (PDI = 0.2)	192.36 ± 1.9 (PDI = 0.2)	360.33 ± 8.0 (PDI = 0.2)
7	215.83 ± 7.7 (PDI = 0.2)	167.26 ± 0.4 (PDI = 0.4)	198.26 ± 2.7 (PDI = 0.2)	498.30 ± 17.9 (PDI = 0.2)
8	243.26 ± 1.7 (PDI = 0.5)	167.46 ± 3.5 (PDI = 0.3)	185.73 ± 6.5 (PDI = 0.2)	546.73 ± 21.9 (PDI = 0.2)
9	322.63 ± 12.5 (PDI = 0.5)	194.63 ± 1.7 (PDI = 0.3)	180.23 ± 3.5 (PDI = 0.2)	562.13 ± 10.6 (PDI = 0.2)
10	374.06 ± 11.5 (PDI = 0.4)	211.06 ± 3.2 (PDI = 0.3)	173.56 ± 3.8 (PDI = 0.2)	600.00 ± 2.4 (PDI = 0.1)
11	505.50 ± 11.8 (PDI = 0.4)	378.43 ± 22.7 (PDI = 0.4)	195.96 ± 6.5 (PDI = 0.5)	612.23 ± 12.8 (PDI = 0.2)
12	560.33 ± 10.1 (PDI = 0.4)	435.40 ± 48.3 (PDI = 0.4)	241.53 ± 4.6 (PDI = 0.4)	647.60 ± 7.1 (PDI = 0.2)
13	556.90 ± 17.5 (PDI = 0.4)	462.93 ± 6.2 (PDI = 0.3)	346.43 ± 13.9 (PDI = 0.5)	665.36 ± 3.1 (PDI = 0.1)

14	650.70 ± 7.2 (PDI = 0.3)	476.10 ± 29.5 (PDI = 0.4)	507.50 ± 14.0 (PDI = 0.4)	654.36 ± 15.4 (PDI = 0.2)
15	645.90 ± 35.1 (PDI = 0.4)	513.13 ± 20.3 (PDI = 0.4)	562.90 ± 15.5 (PDI = 0.3)	646.86 ± 12.9 (PDI = 0.1)
16	649.70 ± 27.4 (PDI = 0.3)	562.56 ± 42.2 (PDI = 0.3)	627.16 ± 13.7 (PDI = 0.3)	672.50 ± 24.5 (PDI = 0.2)

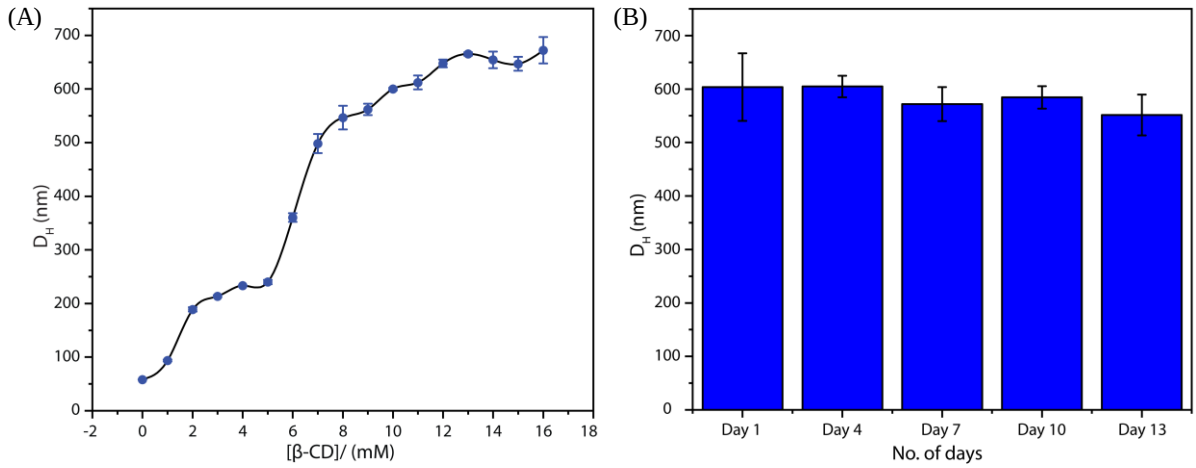

Fig. S6. Variation of hydrodynamic diameter of C12mim:NaOle :: 1:1 system with β-CD addition (A). Stability of composition D over 13 days (B).

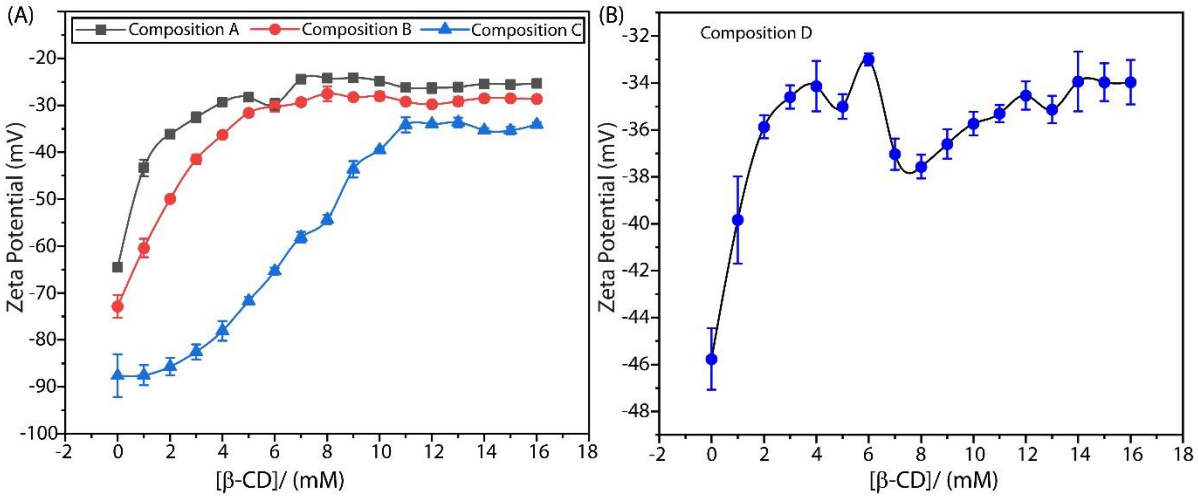

Fig. S7. Variation of zeta potential of different catanionic systems across different concentrations of β-CD.

5. Stability of suprasomes:

As previously noted, suprasomes containing 10 mM of β-CD were prepared. After each day, the hydrodynamic diameter was tested to determine if there had been any size growth, which would indicate aggregation. Thus, a stable hydrodynamic diameter over several days indicated the stability of composition A.

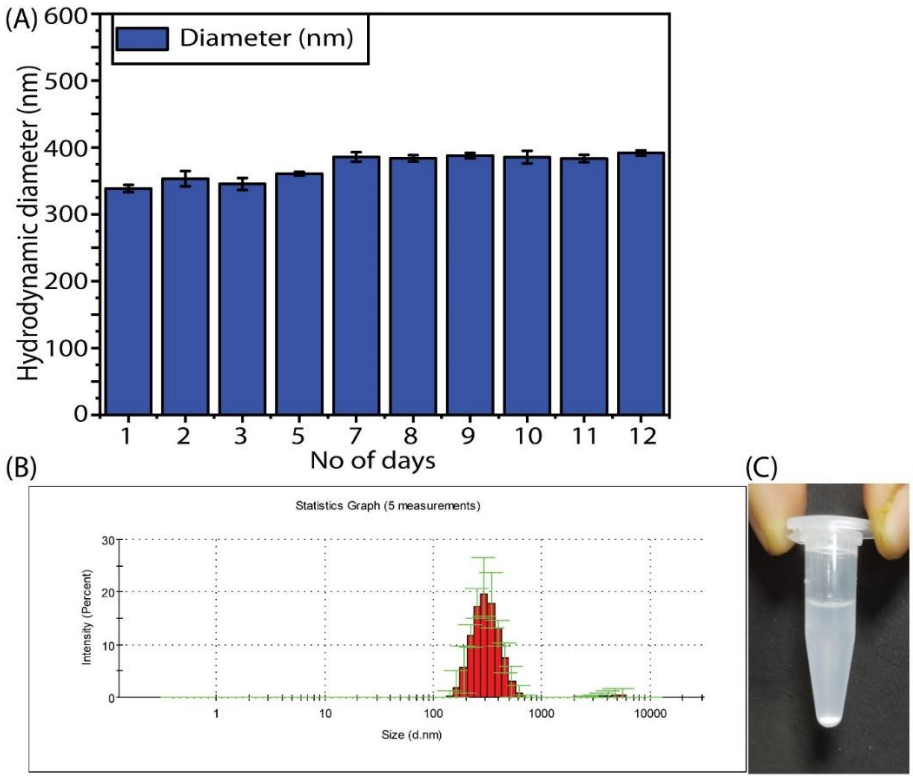

Fig. S8. Variation of hydrodynamic diameter of the soluble aggregates on different days (A). Hydrodynamic diameter measurement of upper solution of composition A after 3 months (B). Visual observation of composition A after 3 months (C).

Note: The β-CD-mediated aggregate transition was also observed visually. The aqueous solutions of C12mbm and NaOle without or with a low concentration of β-CD were transparent at room temperature. However, the solution appeared slightly blueish when the concentration of β-CD was >8 mM, suggesting the increase in the size of the soluble aggregates, which shows light scattering properties (Fig. S1). We hypothesize that this change in average d_H values of the catanionic amphiphiles in the presence of β-CD could be due to micelles-vesicle transition.[1, 2]

Stability in PBS buffer, LB media, and in 5% blood serum — The stability of suprasomes in PBS buffer (pH 7.4), LB media, and blood serum was also investigated by DLS

measurements. PBS and LB media of 1/3rd volume were added to the suprasome solution keeping β-CD concentration fixed at 10 μM, and the D_H values were measured using DLS till 24 h. The suprasomal solutions were also prepared in PBS solution completely, and the D_H were measured over time, suggesting stability of the system as the D_H remained almost constant over 24h. Additionally, we also performed stability tests in blood serum. In this case, stability was observed till 6 h, and eventually, the size started to increase, suggesting a destabilization over a longer time period of 24 h. We would like to mention that careful integration of polyethylene glycol (PEG) can definitely add longer stability to our suprasomal system as it has a well-established reputation for increasing the circulation time of liposomes in the bloodstream, leading to the formation of stealth liposomes.

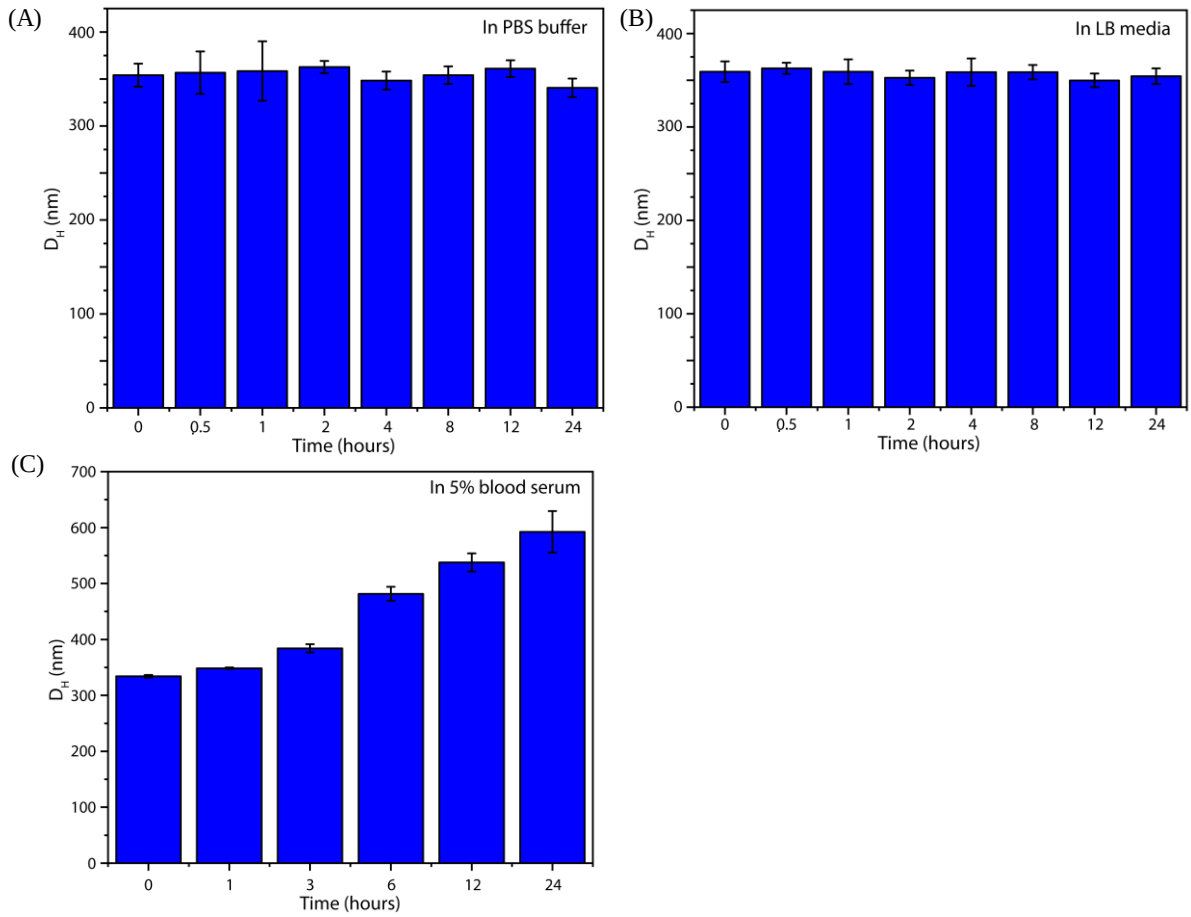

Fig. S9. Stability of composition A in PBS buffer (A), LB media (B), and in 5% blood serum.

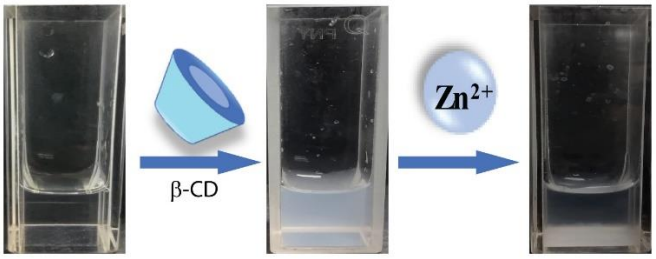

Fig. S10. Visual Change in aggregate transition after β-CD and Zn^{2+}.

6. Isothermal titration calorimetry measurements:

The interaction of β-CD with mixed micelles (C12mbm and oleate) was investigated by isothermal titration calorimetry (ITC) measurements. The heat change induced due to this interaction was measured at 28 °C (301 K) and 350 rpm stirring speed using an ITC-200 microcalorimeter from Microcal (Northampton, MA, USA). The β-CD (0.6 mM) solution was titrated against a 2 mM solution of C12mbm and NaOle (1:1) mixture. The titration method followed 15 injections (2 μL of each) of titrant (C12mbm and NaOle mixture) into the sample cell containing β-CD (200 μL) at 2.0 minutes intervals with continuous stirring. The thermodynamic parameters were determined using a machine running the Microcal Origin 7.0 software. The ΔH and ΔS values were obtained using a nonlinear least-square fit of the data. Gibbs free energy (ΔG) was calculated by using the Gibbs equation: $\Delta G = \Delta H - T\Delta S$. The ΔH and ΔS values suggested this process to be an enthalpy-driven process.

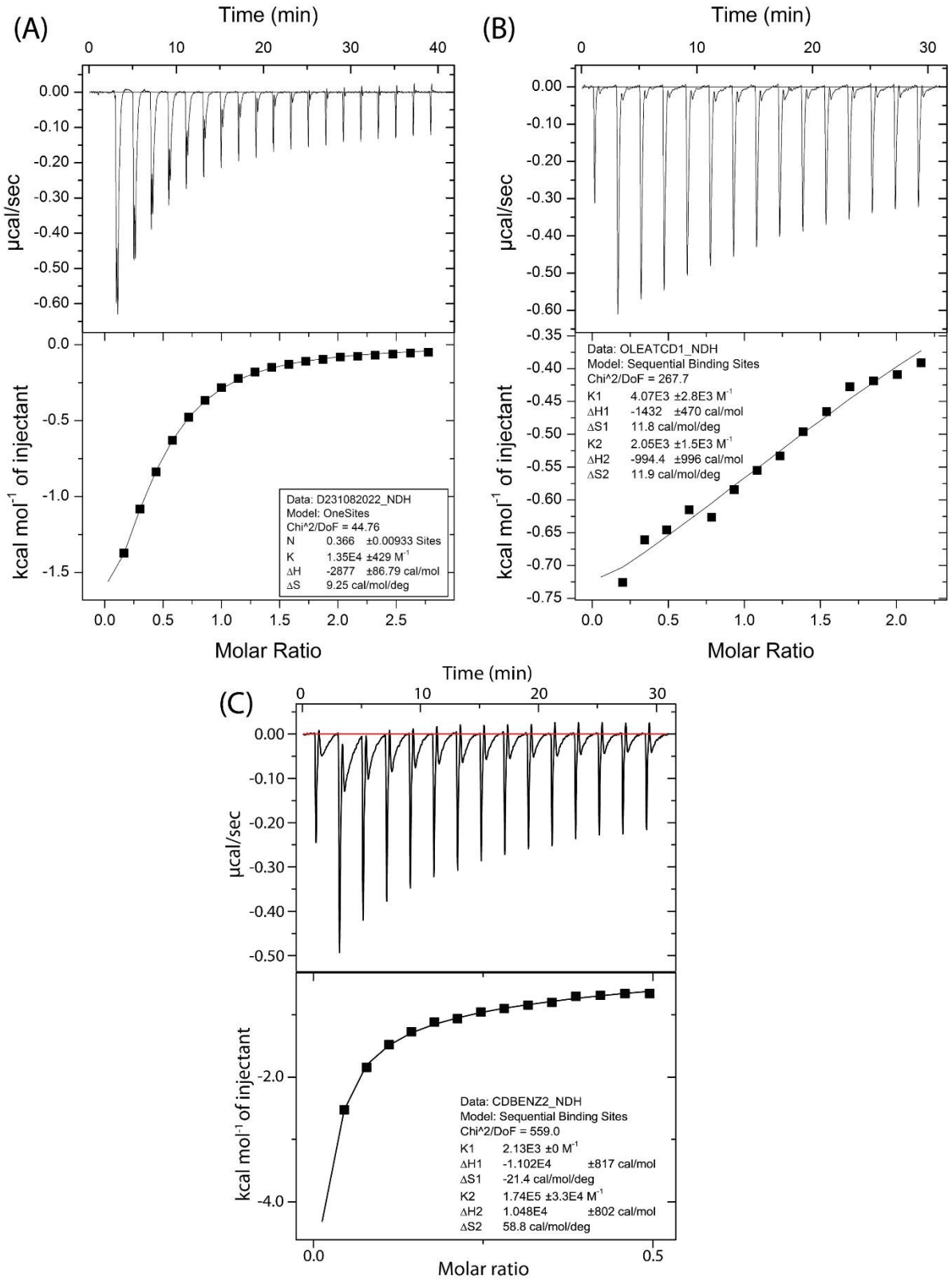

Fig. S11. ITC measurements of the mixture of only C12mbm (A), only NaOle (B) and a mixture of C12mbm and NaOle (1:1) (C) against β-CD.

7. Morphology studies of micelles and suprasomes by TEM and AFM analyses:

Micells and suprasomes solutions were prepared as mentioned above, and FETEM samples were prepared by the drop-cast method. For TEM investigations, 10 μL solution of composition A was placed onto a carbon-coated copper grid and allowed to settle for 5 minutes. After gently blotting the grid with filter paper, the grid was allowed to dry at room temperature for 10 minutes. The grid was then filled with 10 μL of a 2% uranyl acetate solution (in water) and left to dry for an additional minute at room temperature. The grid was dried overnight at room temperature after the extra uranyl acetate solution was soaked out using tissue paper. A JEOL JEM 2100 transmission electron microscope was used to record the images.

For AFM analysis, the samples were prepared by drop-casting 5 μL of micelles and suprasomes solutions onto a silicon wafer. The solution was then allowed to settle for 5 min and soaked with tissue paper. The silicon wafer was dried overnight at room temperature. The AFM images were recorded to determine the morphology of nanoaggregates formed. The samples were imaged by Asylum AFM AC 240 TS-R3 silicon cantilever probes. Topographic images, amplitude, and phase images of the samples were obtained and analyzed by standard AC mode imaging. The Herts model was used to calculate the nanomechanical measurements.

8. Effect of metal ions on hydrodynamic diameter and surface potential:

Suprasomes with composition C12mbm (1 mM), NaOle (1 mM), and β-CD (10 mM) were prepared. The formation of suprasomes of size ~300 nm was confirmed through DLS measurement. Divalent metal ions such as Zn^{2+}, Cu^{2+}, and HCl were added to the suprasome solution with different concentrations (100 μM, 250 μM, 500 μM, 750 μM, 1000 μM) and mixed properly. The hydrodynamic diameters of the nanoaggregates were measured using DLS. The observed increase in size suggested disruption of suprasomes upon trigger and formation of another nanoaggregate.[3] A similar procedure was followed to measure the change in zeta potential upon the addition of divalent metal ions.

Note: Initially, we visualized the formation of a precipitate and a clear solution from the cloudy vesicle solution after adding divalent metals, which suggests the disruption of vesicles (Fig. S8).

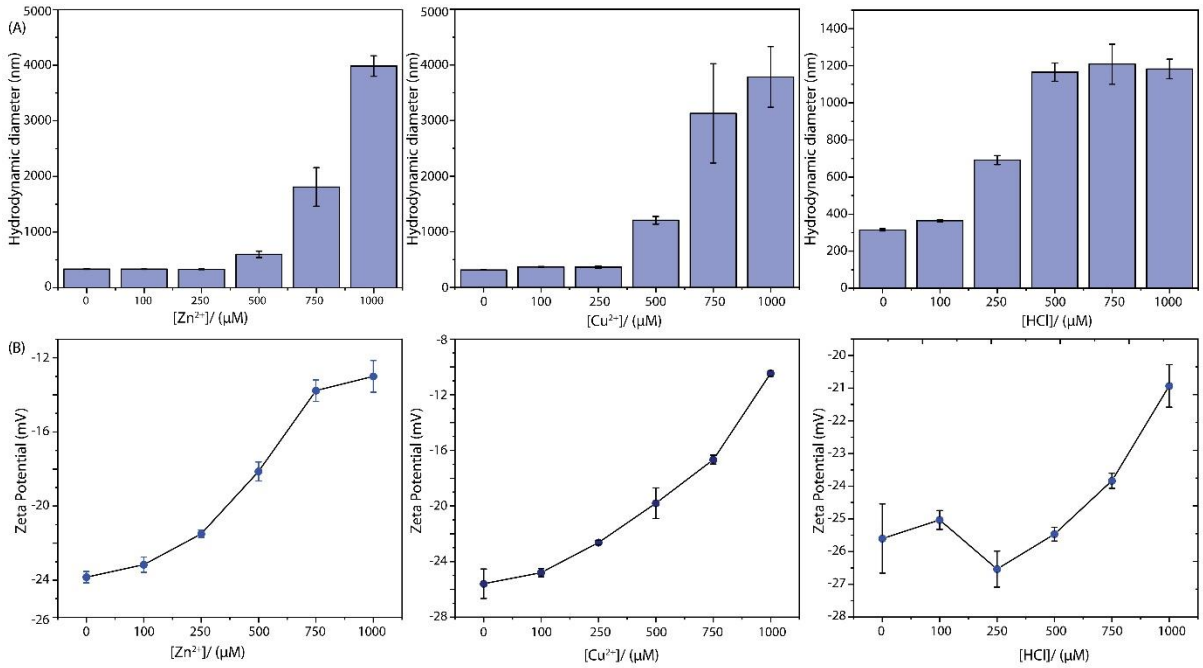

Fig. S12. Variation of hydrodynamic diameter (A) and zeta potential (B) of the suprasomes after treatments with different concentrations of Zn^{2+}, Cu^{2+}, and HCl.

9. Morphology studies of nanoaggregates after Zn^{2+} addition:

The solutions of suprasomes were prepared as mentioned above. To the suprasome solution, $ZnCl_2$ (0.5-1 mM) was added and mixed thoroughly for 10 min. After 15 min, the FETEM and AFM samples were prepared from the above solutions mentioned above.

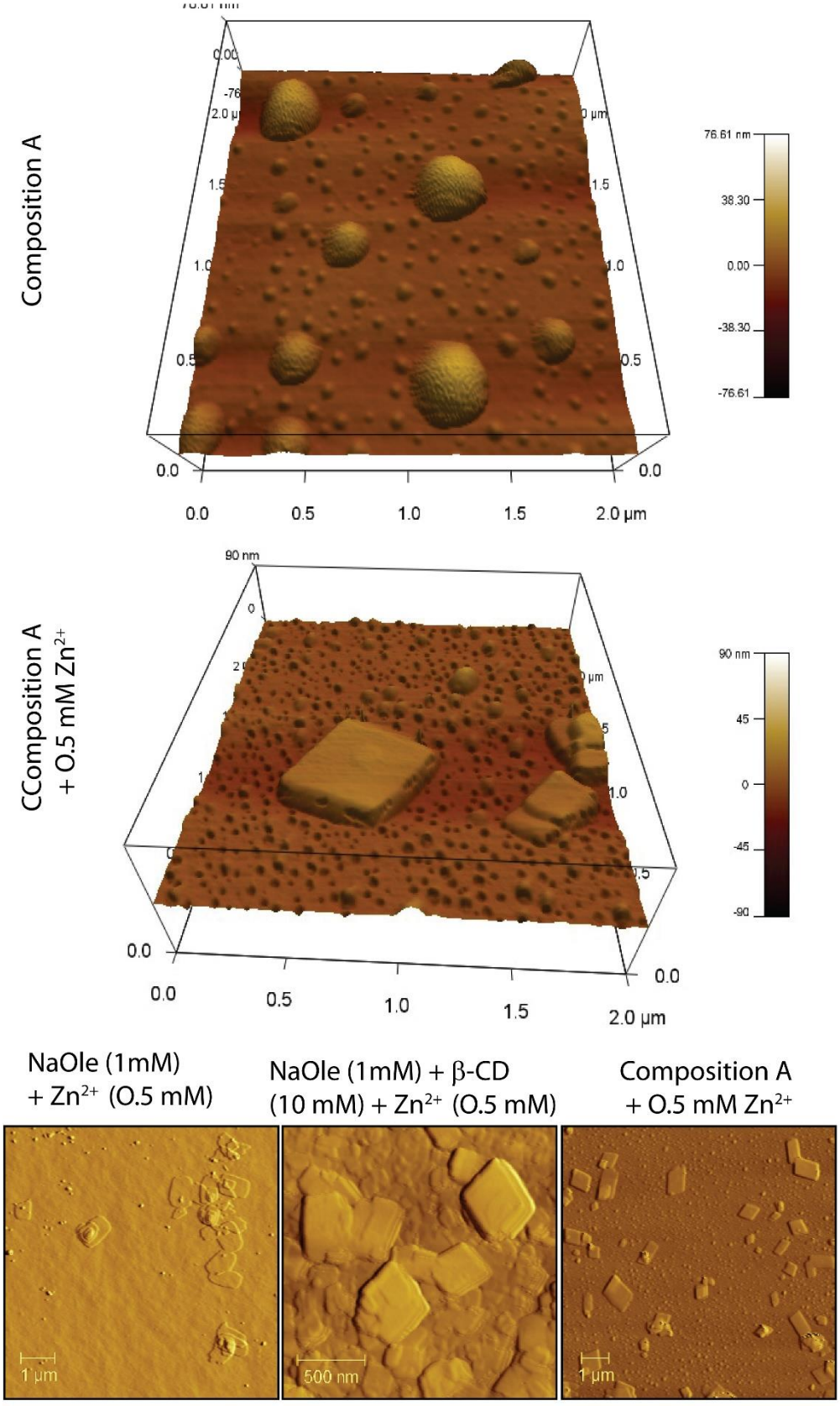

Fig. S13. Change in morphology of suprasomes (AFM images) after Zn^{2+} treatments.

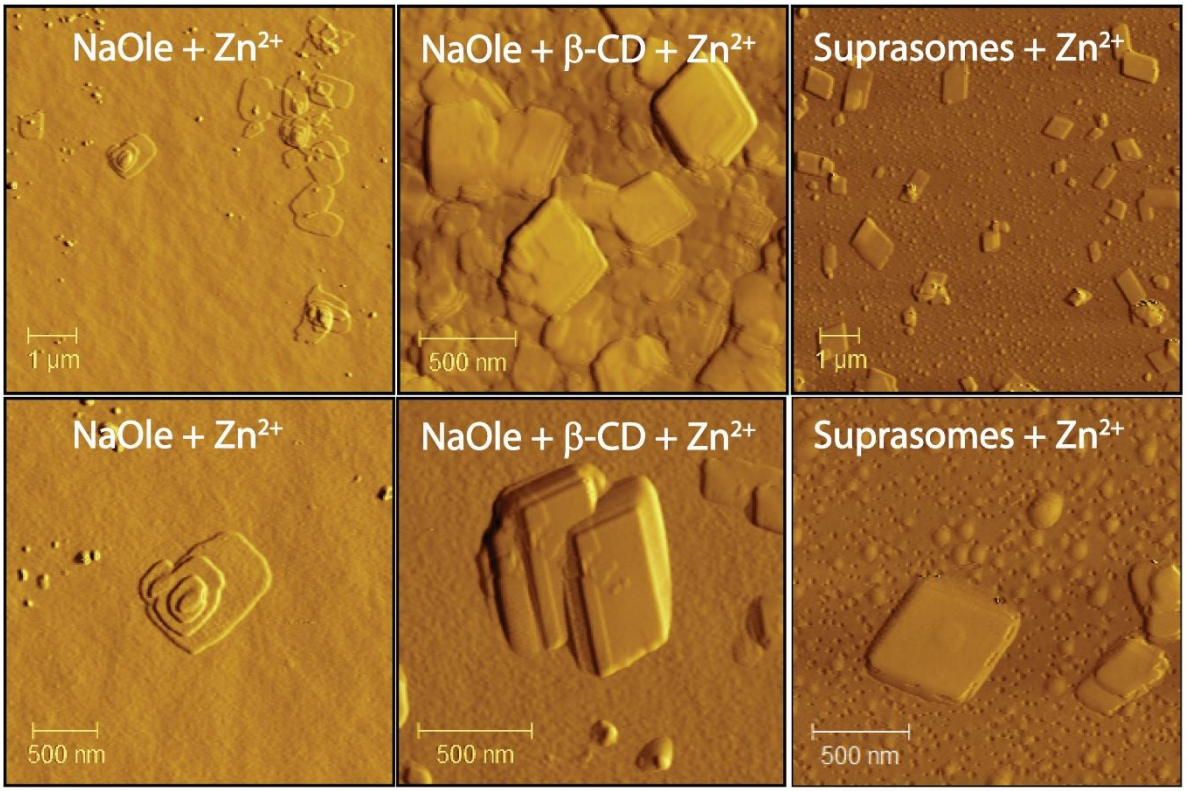

Fig. S14. Change in morphology of NaOle, NaOle + β-CD, and suprasomes after Zn^{2+} treatments.

Note: To investigate the origin of rhombic structures following Zn^{2+} addition to suprasomes, we performed control experiments of NaOle. The addition of Zn^{2+} to NaOle solution resulted in rectangular structures with rounded corners. The addition of Zn^{2+} to the mixture of NaOle and β-CD showed rhombic structures which is comparable to those previously observed in Zn^{2+}-mediated suprasome disruption. These observations indicate that the rhombic structures could be developed from the proper crystalline arrangement of β-CD encapsulated zinc oleate.

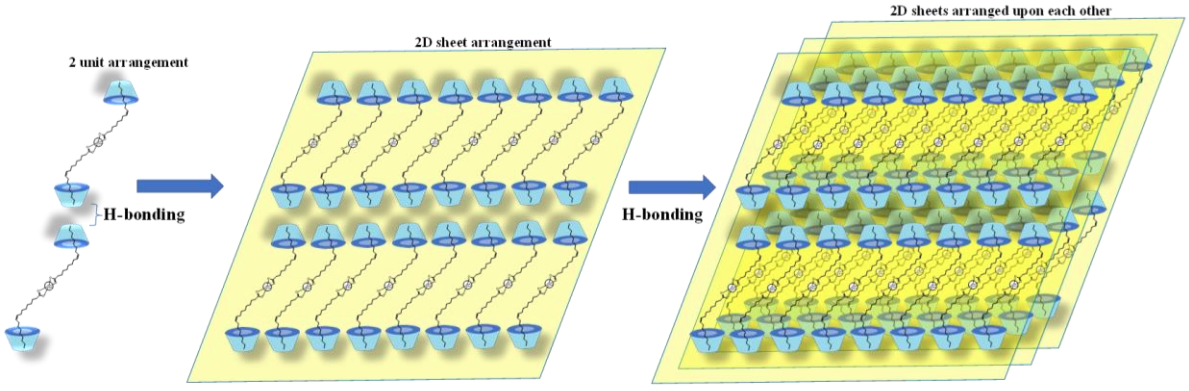

Fig. S15. Probable molecular arrangements of β-CD-Zn-Oleate within the rhombic structure.

10. Nile Red-based kinetics experiment:

Micellar solutions were prepared in an aqueous medium using 1 mM of C12mbm and 1 mM of NaOle, as mentioned above. Nile red was introduced to the mixture at a final concentration of 100 mM, followed by the addition of β-CD (10 mM). The solution was subjected to vortexing for 10 minutes, and then it was shaken overnight at 180 rpm, room temperature, to induce the formation of suprasomes containing Nile red, which was subsequently utilized for the kinetics experiment.

In the kinetics experiment, a 2 mL solution of the suprasomes containing Nile red was exposed to various metals (Zn^{2+}) and acid (HCl) triggers, each at a final concentration of 5 mM, resulting in the swift disruption of the suprasomes. The solution was stirred using a magnetic stirrer till 800 s, and then the stirrer was stopped. The addition of metal and acid triggers caused a decrease in the fluorescence intensity of Nile red (λ_{ex} = 550 nm, λ_{em} = 645 nm), as evidenced by a decrease in the fluorescence signal at 645 nm, suggesting the release of Nile red from the hydrophobic bilayer to the aqueous solution. After adding the metal ions, larger aggregates were observed to have formed, causing a decrease in the fluorescence intensity of the solution. After the stirrer was turned off, these larger aggregates settled gradually, leading to a further decline in the fluorescence intensity of the suprasome solutions.

Note: The NR dye has the propensity to get encapsulated within the hydrophobic layers and shows high fluorescence signal. The disruption of vesicles could lead to the release of NR dye to the aqueous environment and the quenching of the fluorescence signal. This solvatochromic effect serves as an indicator of vesicle disintegration. The low quenching of NR fluorescence intensity after metal addition could be due to the incorporation of NR into other aggregates or within the cavity of the β-CD. A control experiment of NR in the presence of β-CD showed an enhancement of fluorescence intensity. The real-time kinetics experiment with Nile red also revealed the release of solvatochromic dye into an aqueous medium, which significantly reduces fluorescence intensity.

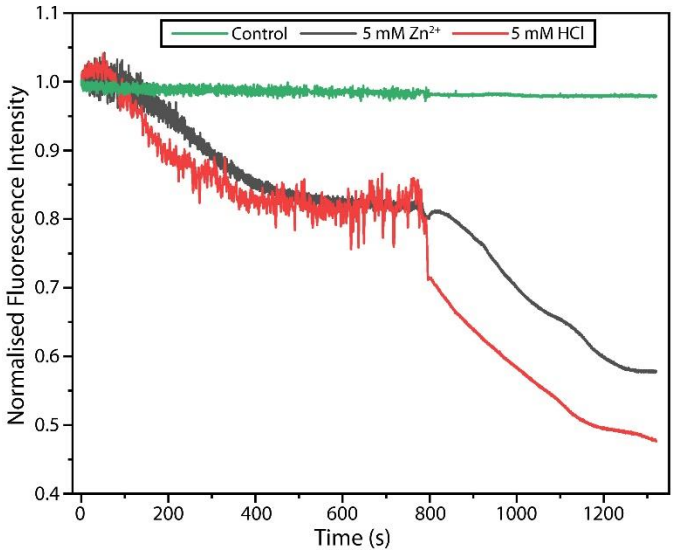

Fig. S16. Stimuli responsive disruption of suprasomes was investigated by time-dependent Nile red assay.

11. Drug encapsulation and release studies:

Tetracycline was used as a model drug to investigate the encapsulation efficacy and release profile of the suprasomes. The tetracycline was added to a micellar solution of C12mbm (1 mM) and NaOle (1 mM) at various doses (50 µM, 200 µM, 400 µM, 800 µM). For improved drug encapsulation, while the suprasomes were developed from micelles, β-CD (10 mM) was added to the solution, sonicated, vortexed for 5 min., and maintained overnight in a shaker at 180 rpm. Ultrafiltration tubes of 10 kD cut-off were used to separate the suprasomes formed, and the drug present in the remaining solution was measured by UV-Vis spectroscopic measurement. This gave us the drug encapsulation efficiency of the suprasomes.

Tetracycline (400 µM) was used for encapsulation in the suprasomes as mentioned above and dialyzed against an aqueous solution in a dialysis bag for 4-6 h until no further excess drug release occurred. Then the dialysis bag was placed in a 40 mL aqueous solution with 0.5 mM Zn^{2+} concentration. At different time intervals, 600 µL solution was removed for measurement and replaced with a fresh aqueous solution. The drug release profile was also measured in the presence of PBS buffer at pH 6.0 following the above procedure.

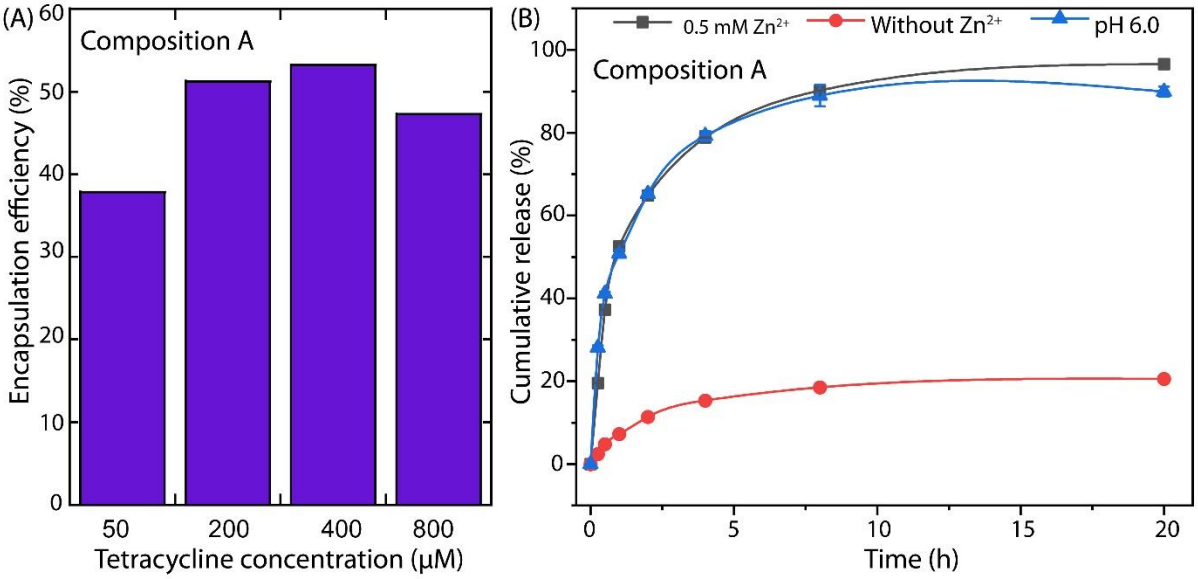

Fig. S17. Tetracycline encapsulation efficacy (A) and release profiles (B) of suprasomes of composition A.

Note: Recent findings revealed that bacterial infections induce low pH environments at bacterial-infected sites, facilitating site-selective drug release.[4] This observation suggests that our suprasome-based DDSs might exhibit effectiveness in bacterial-infected regions characterized by a low pH environment.

12. Antimicrobial activity assessment:

The antimicrobial activity of the additives (C12mbm, C12mim, and different compositions) was assessed by micro-broth dilution method against the MTCC-acquired gram-positive bacterial cells *Staphylococcus aureus* (*S. aureus*; MTCC-96). The Glycerol stock of the bacterial culture was streaked onto the agar plate containing the Luria Bertani (LB) media. A single colony was inoculated into broth media and allowed to grow till mid logarithmic phase at 37 ºC, 180 rpm in a shaker incubator. In a 96-well plate, additives were sequentially diluted in PBS supplemented with 4 % DMSO.

Using the micro broth dilution method, the antibacterial efficacy of the compounds was assessed against gram-positive (*S. aureus* and MRSA) and gram-negative strains (E. coli). A compound's MIC was calculated as its lowest concentration at which visible growth of the microorganism was inhibited. At 37 °C and 180 rpm, the bacteria were grown in an LB medium (Luria Bertani Broth). As soon as the desired optical density had been attained, the bacteria were centrifuged and washed with distilled water before being diluted to 106 CFU/mL in an LB medium. Serial dilution of the compound was performed in a 96-well plate using a

micropipette. The cells were added to the serially diluted solution of the compound and incubated at 37 °C for 14-16 hours. Following incubation, the OD600 was measured with a BioTek Epoch microplate reader to determine the MIC. In order to obtain the most accurate MIC values, this assay was repeated at different concentration ranges.

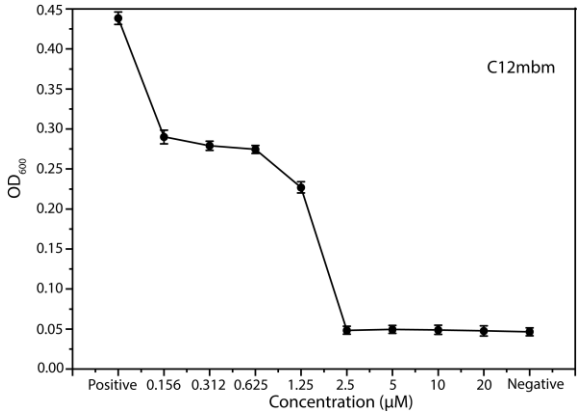
C12mbm
OD600
Positive 0.156 0.312 0.625 1.25 2.5 5 10 20 Negative
Concentration (μM)

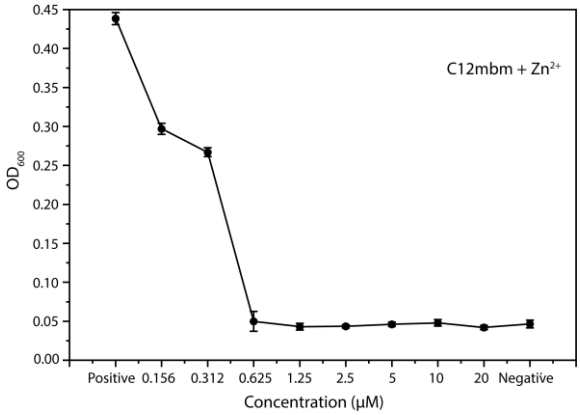
C12mbm + Zn2+
OD600
Positive 0.156 0.312 0.625 1.25 2.5 5 10 20 Negative
Concentration (μM)

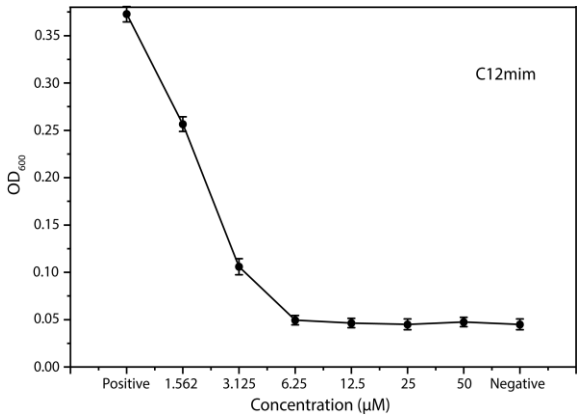
C12mim
OD600
Positive 1.562 3.125 6.25 12.5 25 50 Negative
Concentration (μM)

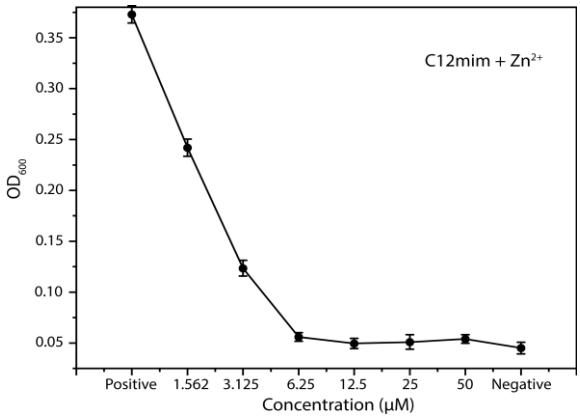
C12mim + Zn2+
OD600
Positive 1.562 3.125 6.25 12.5 25 50 Negative
Concentration (μM)

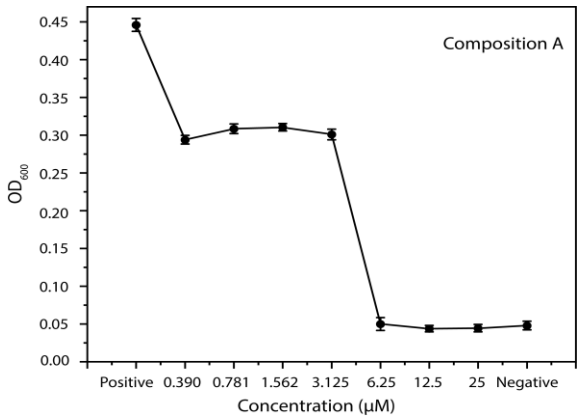
Composition A
OD600
Positive 0.390 0.781 1.562 3.125 6.25 12.5 25 Negative
Concentration (μM)

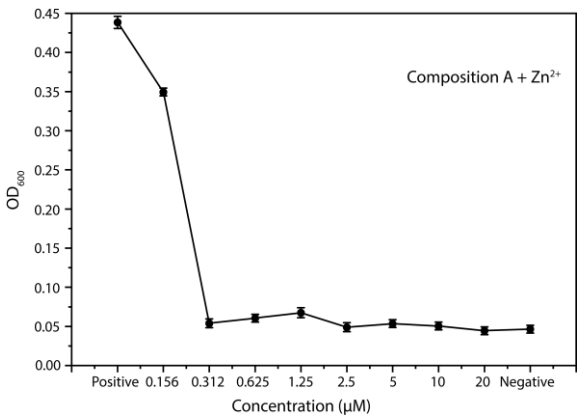
Composition A + Zn2+
OD600
Positive 0.156 0.312 0.625 1.25 2.5 5 10 20 Negative
Concentration (μM)

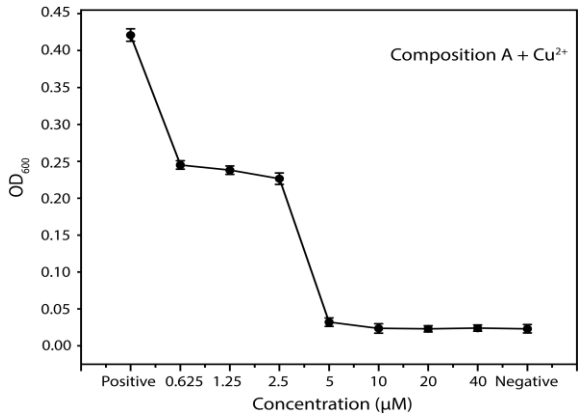
Composition A + Cu2+
OD600
Positive 0.625 1.25 2.5 5 10 20 40 Negative
Concentration (μM)

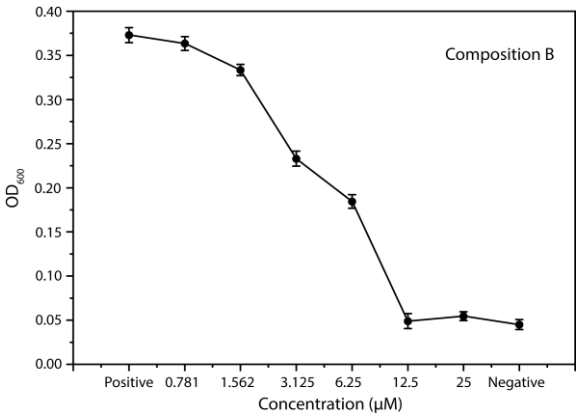
Composition B
OD600
Positive 0.781 1.562 3.125 6.25 12.5 25 Negative
Concentration (μM)

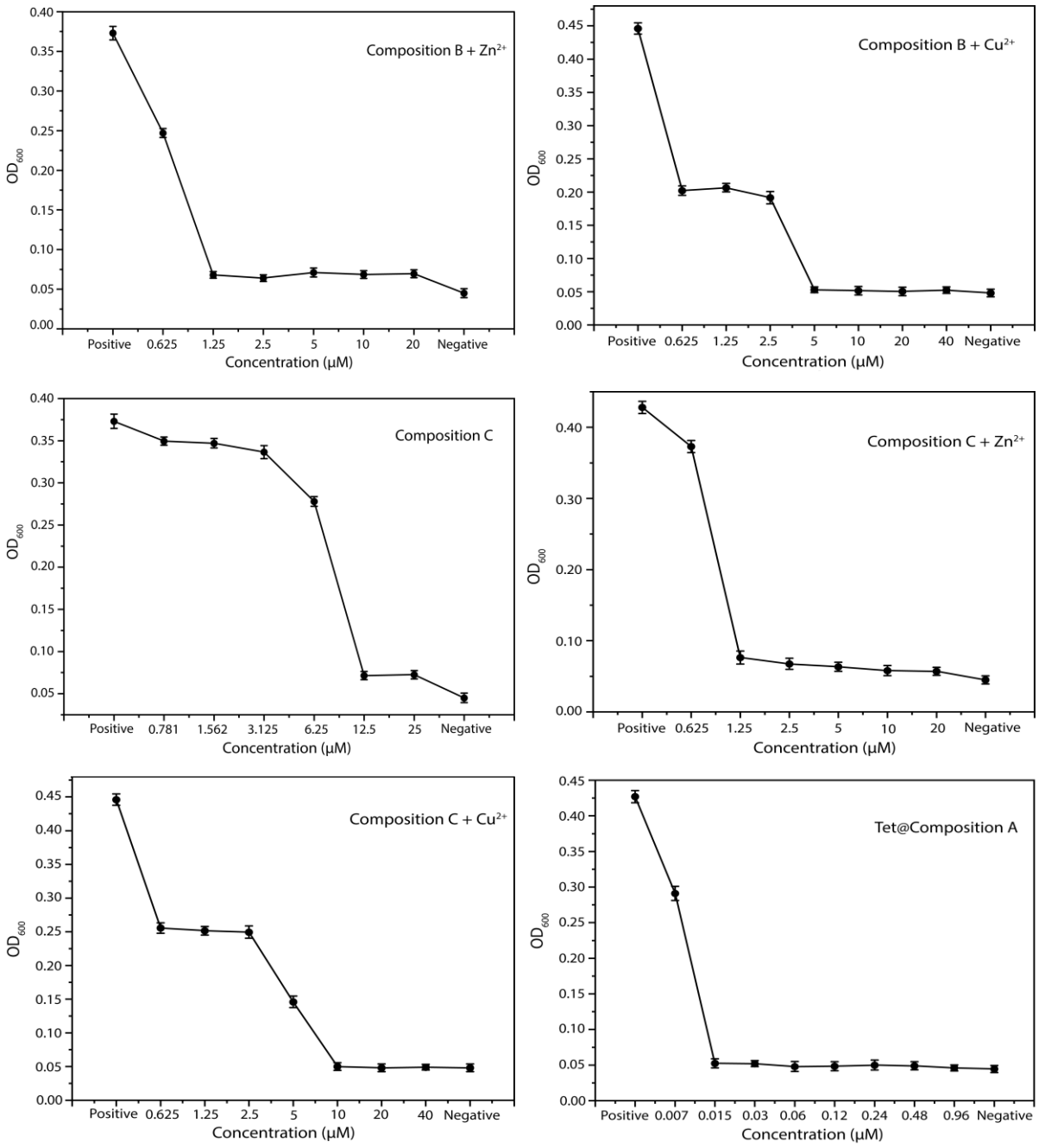

Figure S18. OD_{600} vs concentration plot of different additives for *S. aureus* bacterial cells.

Table S3. Calculated MIC values of the additives against different bacterial strains.

Composition	MIC (μM)		
	S. aureus	MRSA	*E. coli*
C12mbm	2.50 ± 0.5	10 ± 1.0	20
C12mbm + Zn^{2+} (250 μM)	0.62 ± 0.1	2.5 ± 1.5	
Composition A	6.25 ± 1.0	5.0 ± 0.5	20
Composition A + Zn^{2+} (250 μM)	0.31 ± 0.1	2.5 ± 1.5	

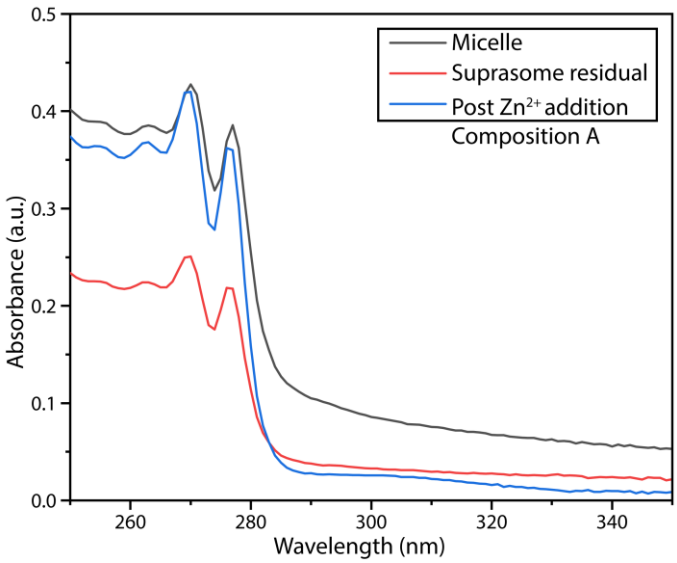

Fig. S19. Absorbance spectra of free C12mbm before and after treatments.

Note: Further analysis revealed that the antibacterial activity of suprasomes in the absence and presence of Zn^{2+} could be due to the abundance of free C12mbm under experimental conditions. To quantity the free C12mbm, either in its micellar state or entrapped within suprasomes, we performed UV-Vis spectral analysis across three distinct conditions: firstly, in its original micellar form; secondly, following the addition of beta-cyclodextrin (β-CD) facilitating suprasome formation; and lastly, when Zn^{2+} was introduced for disruption of suprasomes. This experimental investigation revealed a compelling relationship between suprasome formation induced by β-CD and the sequestration of C12mbm within the suprasomes, where the encapsulation of alkyl long chain of C12mbm occurs by β-CD molecules. Simultaneously, during suprasome formation charge of free benzimidazolium will be masked by excess free oleate, as shown, leading to the overall masking property. The Zn^{2+} triggered disruption of the suprasomes, resulting in the liberation of C12mbm. Remarkably, the observed behavior was intimately connected to the antibacterial efficacy exhibited by the micellar system, the suprasomes, and the system after Zn^{2+}-triggered disruption.

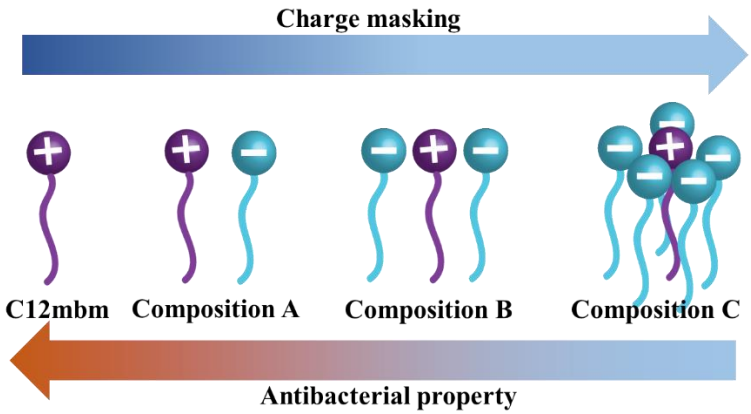

Fig. S20. Charge masking of free C12mbm by free NaOle.

13. Bacterial cell morphology analysis by FESEM:

For morphological analysis of the additive-treated bacterial cells, *S. aureus* cells were treated as in the aforementioned sections until the mid-logarithmic phase. Cells were harvested and treated with the compound at its MIC value. After the incubation at 37 ℃, 180 rpm cells were centrifuged, and the palate was resuspended in the buffer and treated with 3% glutaraldehyde for 30 min to fix the cells. Bacterial cells were again centrifuged to wash the cells and incubated in Milli-Q water. For the analysis, 10 µL of the sample was mounted onto a glass grid and allowed to dry under laminar airflow. Before the analysis sample containing glass, the grid was stacked onto the FESEM grid and coated with gold.

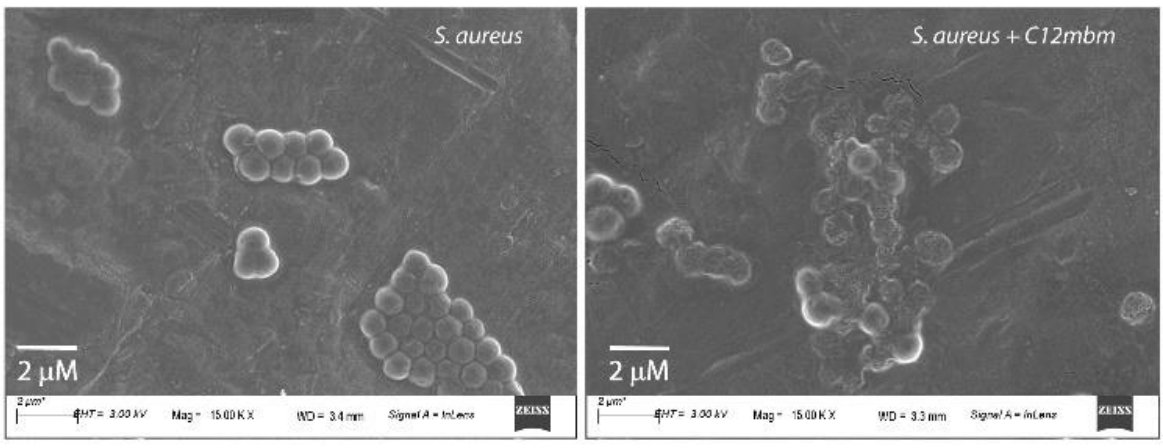

Fig. S21. Representative FESEM images of untreated and **C12Mbm** treated *S. aureus* cells.

14. Blood cells cytocompatibility test:

Biocompatibility of the benzimidazolium containing β-CD compositions was performed against fresh erythrocytes human blood as per our earlier reported protocol and as per the guidelines of the Institutional Human Ethics Committee (IHEC). Before assay, blood was centrifuged to separate the plasma from erythrocytes at 1500 rpm for 5 min and washed twice with buffer at 7.4 pH (20 mM HEPES, 100 mM NaCl). 5% hematocrit was prepared. Serially diluted different compounds were prepared in the same buffer, and for the negative control, only buffer was taken, while for positive control, detergent (0.1 % Triton-X) was taken for complete cell lysis. To the serially diluted samples, hematocrit was added and incubated at room temperature for 1 hr. After incubation, the sample vial was centrifuged, and 200 µL of the supernatant from the sample vials was aliquoted into 96-well plates, and its absorbance was measured at 410 nm by using a plate reader (Biotech).[5] The hemolytic assessment was made by comparing the absorbance of the samples with negative and positive control.

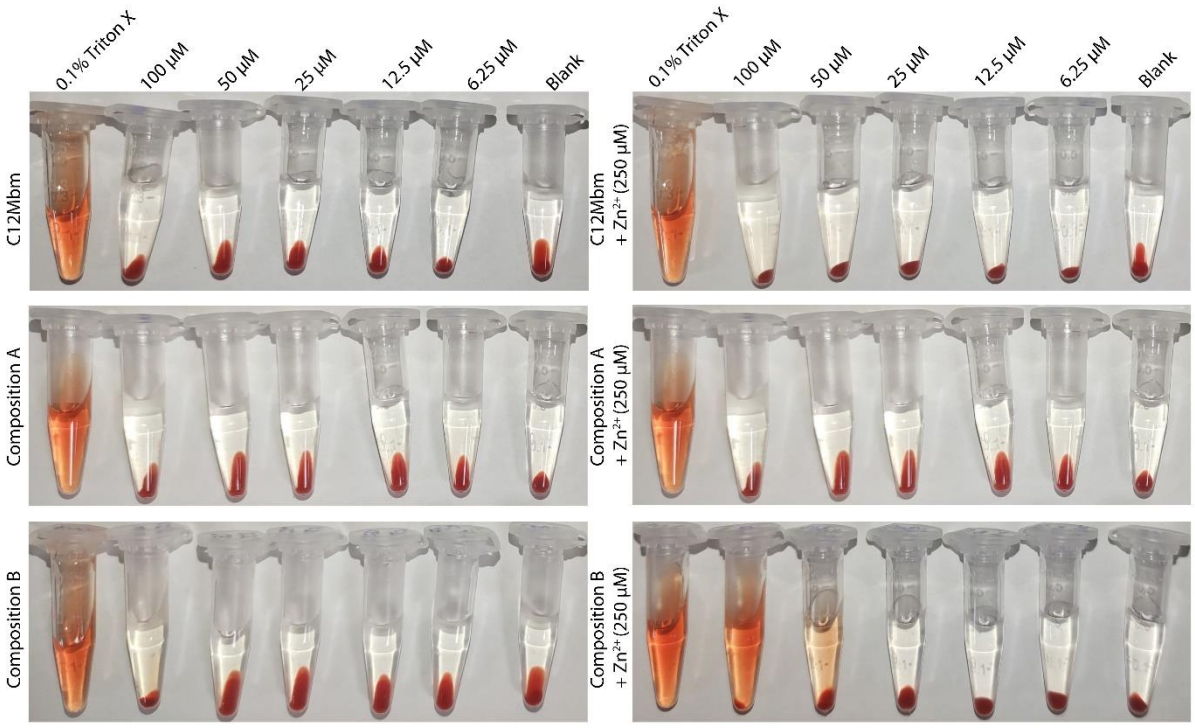

Fig. S22. Extent of hemolysis of C12mbm, Composition A and Composition B.

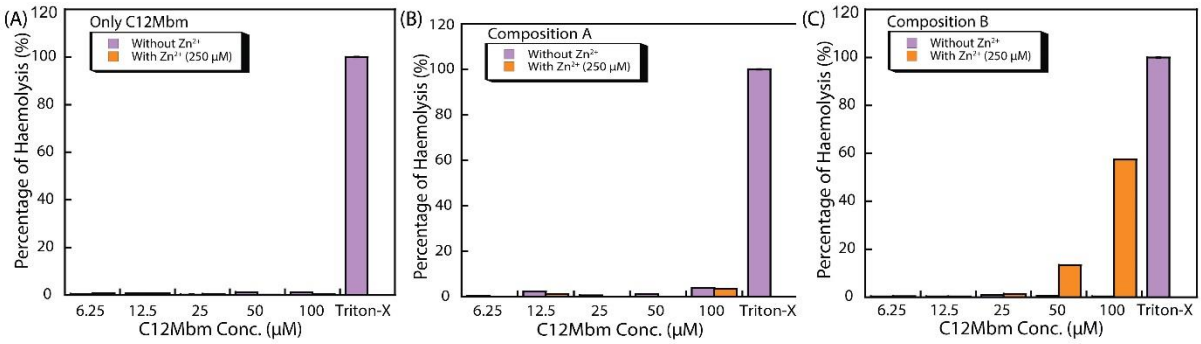

Fig. S23. Percentage of hemolysis of C12mbm (A), Composition A (B), Composition B (C).

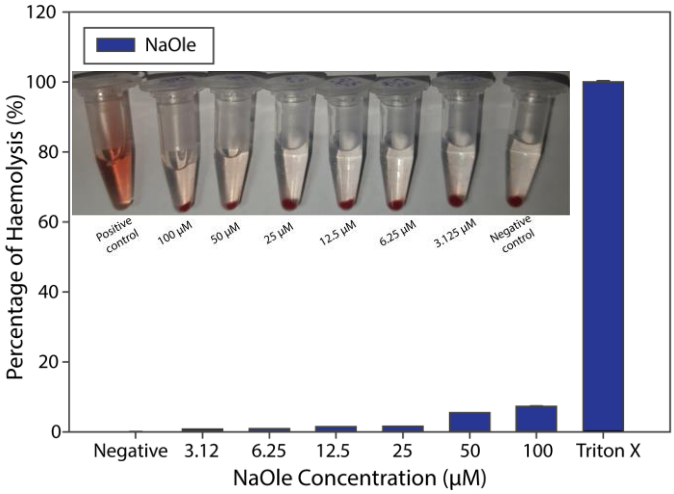

Fig. S24. Extent of hemolysis of NaOle.

15. Cell viability assay:

The cellular cytotoxicity of the compounds was assessed by the standard 3-[4,5-dimethylthiazol-2-yl]-2,5-diphenyl tetrazolium bromide (MTT) assay on the HEK293 cell line. Approximately 10^5 cells/well (per 100 µL) were seeded in 96-well flat-bottom tissue culture plates and grown in media containing 10% fetal bovine serum (FBS) in Dulbecco's Modified Eagle Medium (DMEM) and incubated at 37°C in 5% CO2 pressure. After 12-16 h, the media was discarded, and each well was washed with phosphate-buffered saline (PBS), followed by the addition of the serially diluted compounds in plain DMEM media without FBS to each well and incubated for 24h at 37°C in 5% CO_2 pressure. Following, 100 µL of fresh plain DMEM medium with MTT (5 mg/mL) were added to wells and incubated for another 2 h at 37°C. The MTT-containing medium was removed from each well, and the formazan crystal formed was solubilized in 100 µL, and absorbance was recorded on a microplate reader (Multiskan™ GO) at the wavelength of 570 nm. All experiments were performed in triplicate, and the relative cell viability (%) was expressed as a percentage relative to the untreated cells.

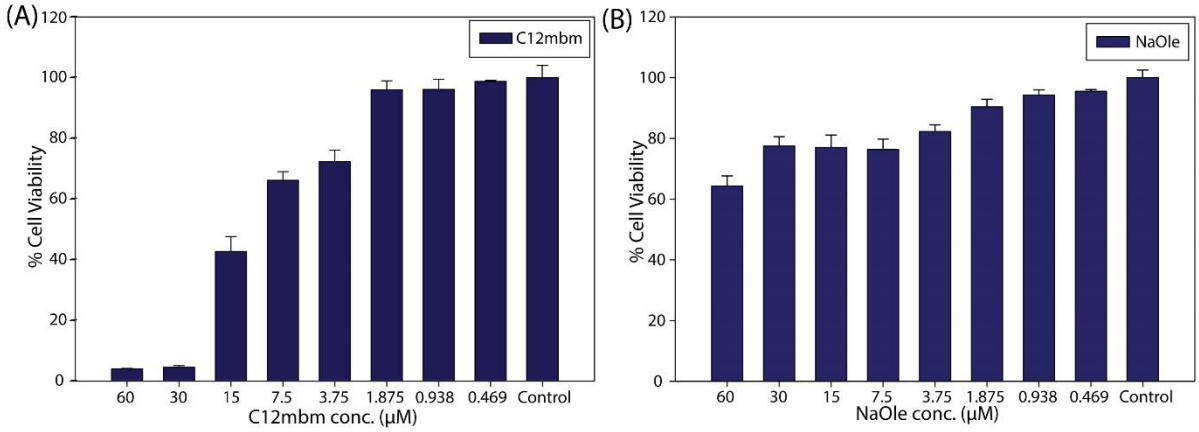

Fig. S25. Percentage of cell viability in the presence of different concentrations of C12mbm (A) and NaOle (B) after 24 h of treatments.

Note: The IC_{50} value of C12mbm was found to be 12.57 µM. The results indicated that C12mbm exhibits biocompatibility at concentrations 20-30 times higher than the MIC value of tetracycline@composition A. Although C12mbm showed cytotoxicity against normal cell lines, its antibacterial effect was achieved at very low concentrations, which could be due to the synergistic effect of C12mbm, Zn^{2+}, and tetracycline. The combined action of these components enhances the antimicrobial efficacy of the system, allowing for effective antibacterial activity at significantly reduced concentrations of C12mbm. These findings highlight the potential of our developed system for targeted antibacterial applications, where low concentrations can achieve the desired therapeutic effects while maintaining biocompatibility.

All the experiments related to hemolysis and HEK293 cell lines were carried out in compliance with the Institutional Human Ethics Committee (IHEC) Guidelines, and the experiments were authorized by the Indian Institute of Technology Guwahati's ethics committee. Informed consents were obtained from the human participants of this study. The HEK-293 cell lines were obtained from National Centre for Cell Science (NCCS).

16. Membrane depolarization assay:

Membrane depolarization assay was performed against *S. aureus* cells which were grown in LB broth at 37 °C, 180 rpm, till the mid-logarithmic phase. The cells were collected by centrifugation at 5000 rpm for 3 mins. After resuspending the bacterial pellet in HEPES buffer (10 mM HEPES in 50 mM glucose), $DiSC_3(5)$ dye (membrane depolarization sensing dye) at

0.4 µM final concentration was added, and cells were incubated at 37 °C for 1 hour. Thereupon, 100 mM KCl was added, followed by 15 mins of incubation. Afterward, varied compound concentrations (0, 5, and 10 µM) were added to the cell suspension along with 10 µM valinomycin as a positive control. The fluorescence spectra of cell suspensions were recorded (λ_{ex} = 620 nm, λ_{em} = 650 nm).

17. Propidium iodide uptake assay:

The propidium iodide (PI) uptake assay was performed to assess the membrane integrity of bacteria in the presence of compounds. The previously outlined methodology was used to culture and harvest *S. aureus* cells.[6] After resuspending the bacterial pellet in PBS buffer, the compound was added to the cell suspension at a concentration equivalent to its MIC value. The cells were also resuspended in the buffer for the control. Furthermore, the cells were incubated at 37°C, 180 rpm. After sampling at different time intervals (0.5, 1, and 2 hrs), samples were centrifuged and resuspended in the buffer. After that, it was treated with PI (30 µM) for 30 minutes. Unbound dye was removed through centrifugation, and the bacterial cells were resuspended in the buffer. The fluorescence spectrum of the samples was recorded after a certain period of time (λ_{ex} = 535 nm, λ_{em} = 610 nm).

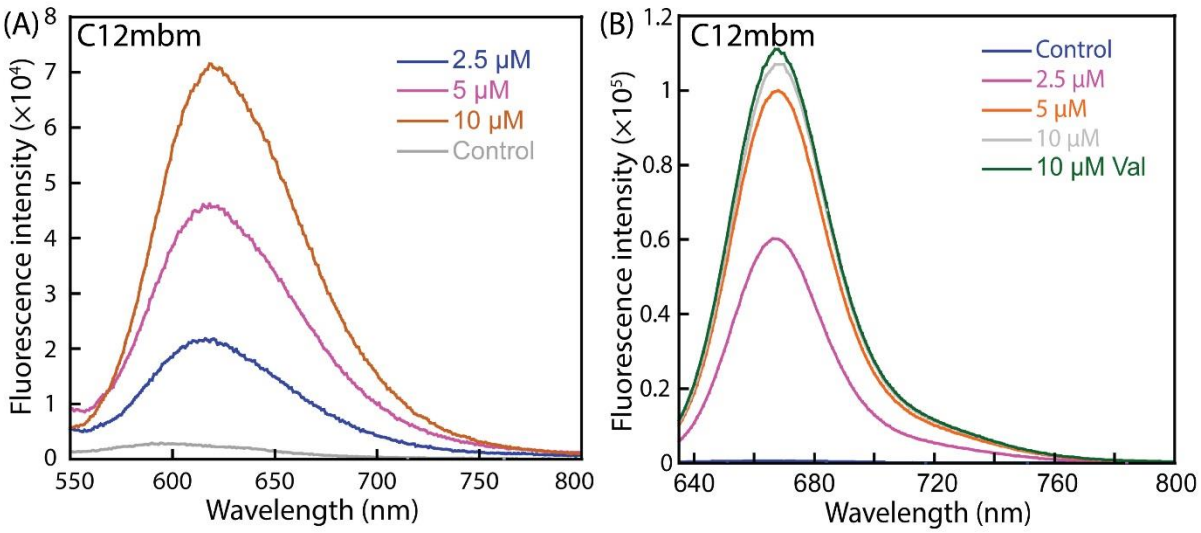

Fig. S26. Fluorescence-based PI uptake (A) and membrane depolarization (B) studies of C12Mbm treated *S. aureus* cells. Val = Valinomycin.

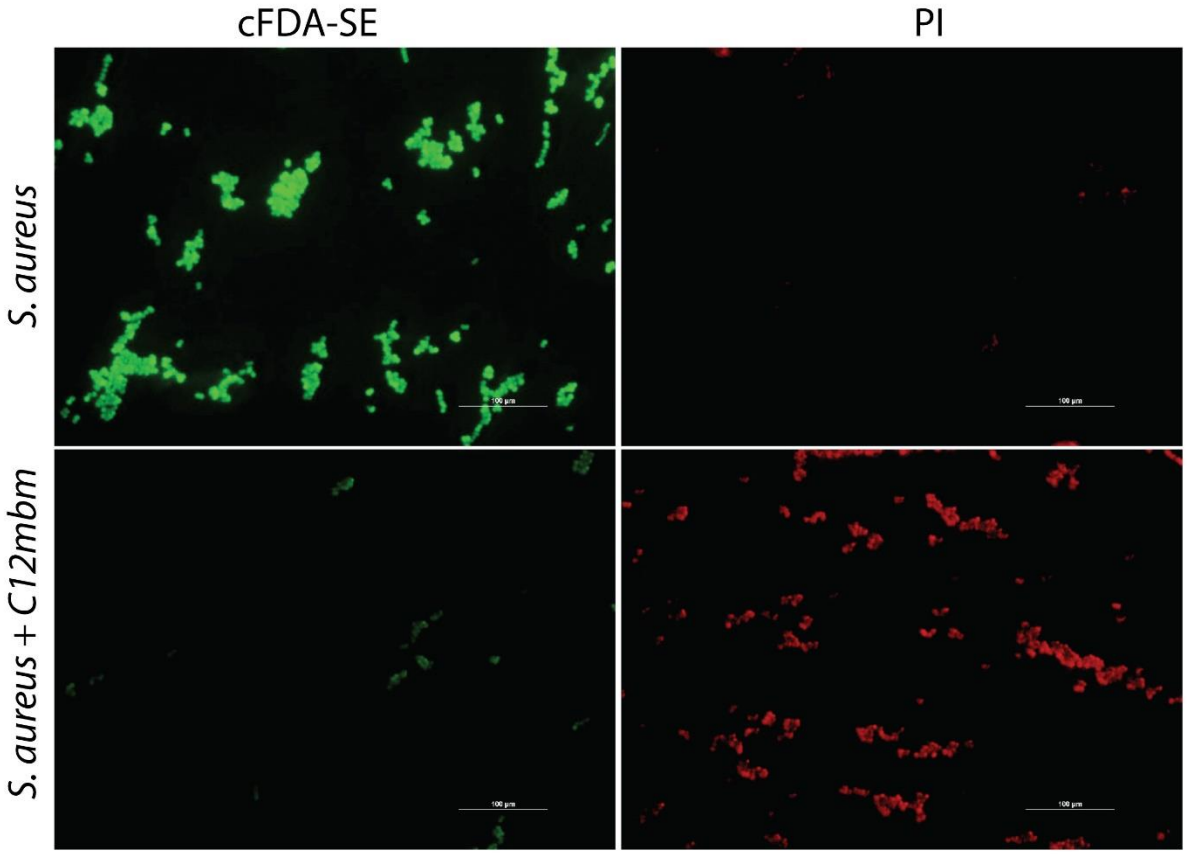

Fig. S27. Microscopic images of PI uptake and membrane depolarization studies of C12Mbm treated *S. aureus* cells.

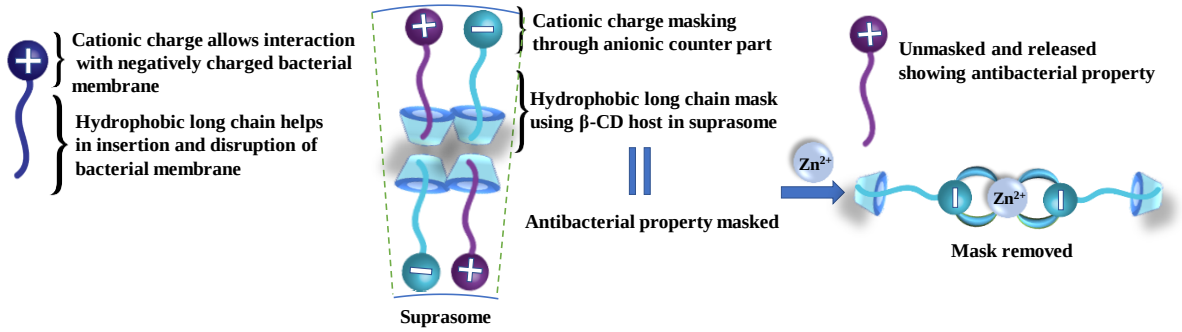

Fig. S28. Plausible explanation for the masking and unmasking of cationic charge.

Note: Metal responsive behavior of suprasome

We also conducted DLS based size increment experiment upon metal ion addition to provide a clear picture of which metal can destabilize the suprasome-based DDSs. The change in D_H values suggested that monovalent metal ions are ineffective in causing any disruption to the suprasome, even at very high concentrations. So we tried to investigate the role of biologically

available divalent metal ions, which can cause suprasome disruption. We scanned through the concentration range of metal ions such as Zn^{2+}, Cu^{2+}, Ca^{2+}, Ni^{2+}, Mg^{2+}, and Fe^{3+} by adding them to the suprasome solution of composition A. The change in D_H values upon these metal ion additions at different concentrations indicates that the Zn^{2+} causes a significant change in hydrodynamic diameter at 400 μM, whereas Cu^{2+} and Fe^{3+} at 500 μM and 700 μM, respectively. Other metal ions such as Ca^{2+}, Ni^{2+}, and Mg^{2+} showed any significant change in D_H at very high concentrations of 5-12 mM. We further investigated the literature reports for the abundance of free metal ion concentration in the body (Blood serum), which were in the range of 10-50 μM range. The concentrations of these metal ions in body fluid (blood serum) were found to be well below the disruptive levels, indicating likely stability in the presence of these metal ions in body fluid. It is important to note that only the free metal ion concentration matters, as most metal ions are bound to certain proteins. Hence the suprasomal system should remain stable in body fluid. Additionally, we provided a table to clarify the change in size with respect to different metals and hope this will add clarity and better comprehension to the readers.

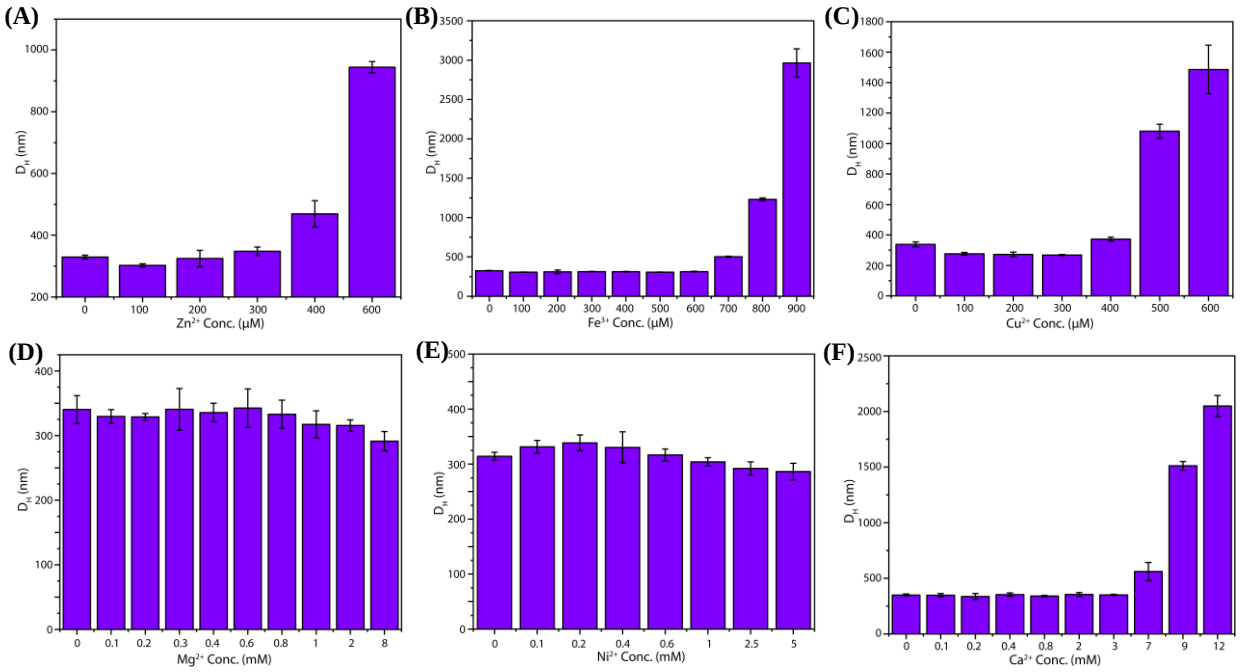

Fig. S29. Metal responsive behavior of suprasome, hydrodynamic diameter at different metal ion concentration, Zn^{2+} (A). Fe^{3+} (B), Cu^{2+} (C), Mg^{2+} (D), Ni^{2+} (E), Ca^{2+} (F).

Table S4. Metal ion concentrations are required for significant destabilization of suprasome.

Metal ions	Concentration required for suprasome disruption (μM)	Concentration of metal ion in blood serum (μM)
Zn^{2+}	400	0.1-2[7]
Cu^{2+}	500	11-24[8]
Fe^{3+}	700	30-40[9]
Ca^{2+}	7000	2500[10]
Mg^{2+}	> 8000	750-1050[11]
Ni^{2+}	> 5000	0.002[12]

Though this study suggested the suprasomes had higher responsiveness to a few metal ions such as Zn^{2+}, Cu^{2+}, and Fe^{3+}, we believe that this can be utilized as an opportunity to get wider applications. We presume that this could be treated as an opportunity to deliver drugs to tissues or pathological conditions where these metal ions (Zn^{2+}, Cu^{2+}, Fe^{3+}) have a high concentration level. We provided a table with the tissues and pathological conditions in the body with high concentrations of these metal ions.

Table S5. Tissues and pathological conditions with very high metal ion concentrations.

Metal ions	Tissues with higher concentration	Pathological conditions with higher concentration
Zn^{2+}	hippocampus, amygdala, cortex, pancreas, and prostate	Prostrate related pathological conditions[13]
Cu^{2+}	Liver, kidney	Wilson's disease[14]
Fe^{3+}	Spleen	Hemochromatosis[15]

18. References

1. C. L. Dai, Z. Yang, H. L. Yang, Y. F. Liu, J. C. Fang, W. X. Chen, W. T. Li and M. W. Zhao, *Colloid Surface A*, 2016, **498**, 1-6.
2. J. E. Yang, H. J. Huang, L. Zhu, H. Xie and F. Gao, *Colloid Surface A*, 2019, **582**.
3. J. C. Lou, J. A. Schuster, F. N. Barrera and M. D. Best, *J Am Chem Soc*, 2022, **144**, 3746-3756.
4. S. L. Cui, J. Qiao and M. P. Xiong, *Mol. Pharmaceutics*, 2022, **19**, 2406–2417.

5. A. Patel, S. Dey, K. Shokeen, T. M. Karpinski, S. Sivaprakasam, S. Kumar and D. Manna, *Rsc Med Chem*, 2021, **12**, 1005-1015.

6. A. Patel, S. Paul, N. Akhtar, S. Das, S. Kar, S. Bhattacharjee and D. Manna, *Acs Appl Nano Mater*, 2022, **5**, 16602-16611.

7. S. K. Gotru, J. P. van Geffen, M. Nagy, E. Mammadova-Bach, J. Eilenberger, J. Volz, G. Manukjan, H. Schulze, L. Wagner, S. Eber, C. Schambeck, C. Deppermann, S. Brouns, P. Nurden, A. Greinacher, U. Sachs, B. Nieswandt, H. M. Hermanns, J. W. M. Heemskerk and A. Braun, *Sci Rep-Uk*, 2019, **9**.

8. B. Blicharska, M. Witek, M. Fornal and A. L. Mackay, *J Magn Reson*, 2008, **194**, 41-45.

9. Y. O. Kim, H. J. Chung, H. S. Kong, D. W. Choi and D. H. Cho, *Arch Pharm Res*, 1999, **22**, 288-293.

10. L. G. R. John P. Bilezikian, T. John Martin, *Principles of Bone Biology, 3rd ed.* , Elsevier, 2008.

11. L. G. R. John P. Bilezikian, T. John Martin, *Principles of Bone Biology, 4th ed.*, Elsevier, 2020.

12. B. A. F. a. M. N. Gunnar F. Nordberg, *Handbook on the Toxicology of Metals, 4th ed.*, Elsevier, 2015.

13. M. L. Zastrow, R. J. Radford, W. Chyan, C. T. Anderson, D. Y. Zhang, A. Loas, T. Tzounopoulos and S. J. Lippard, *Acs Sensors*, 2016, **1**, 32-39.

14. M. C. Linder, L. Wooten, P. Cerveza, S. Cotton, R. Shulze and N. Lomeli, *Am J Clin Nutr*, 1998, **67**, 965s-971s.

15. A. N. Luck and A. B. Mason, *Curr Top Membr*, 2012, **69**, 3-35.